

# POLITECNICO DI TORINO

Master's Degree Course in Mechanical Engineering

Master's Degree Thesis



**Politecnico  
di Torino**



**ENERGY  
CENTER**

## **Scalable Methodology for Solar Potential of Rooftops and Building Environment Based on Shadow Analysis**

### **Supervisor**

Prof. Pierluigi Leone

### **Candidate**

Buğrahan Çoban

### **Co-supervisors**

Prof. Andrea Lanzini

Prof. Romano Borchiellini

Ing. Daniele Salvatore Schiera

Ing. Riccardo Novo

Academic year 2021/2022

## **Abstract**

In the changing world with the ongoing increase in energy demand and relatively the negative effect on the environment through fossil fuels has raised dramatical challenges. As a result of this issue, renewable energy sources are increasingly considered as potential solutions for a sustainable energy production and reduction of negative environmental impact.

In Italy, the need to decrease the country's historical dependence on fossil fuels and supply flows of hydrocarbons caused an irresistible urge to produce green energy. Therefore, in the twentieth century, Italy has become one of the leading countries in the development of green energy production.

Solar energy is one of the major unlimited and clean renewable energy sources that is gradually replacing non-renewable energy sources. This thesis adopts a mixed methodology with an interdisciplinary framework in order to improve the current methodologies of the estimation of solar photovoltaics potentials combining Solar Energy on Building Envelopes and Shadow Analysis. Four days shadow method was implemented in order to detect the shaded areas and to eliminate them from the rooftops. QGIS software and Python language were used to complete the thesis work.

Aosta Valley was selected as a case study and technical potential of PVs is evaluated by estimating shortwave irradiance on suitable rooftops. The analyses were performed by using two different raster resolution on the same area, and finally the comparison between two different resolutions was documented.

## **Acknowledgment**

I would first like to thank my supervisors Professor Pierluigi Leone and Professor Andrea Lanzini for their guidance and feedback throughout this research. Every result described in this thesis was accomplished with the help and support of co-supervisors Daniele Schiera and Riccardo Novo. I would like to extend my sincere thanks to them and foremost to Francesco Petrosino.

I am also grateful to my friends who have always supported me with their existence since the beginning of my master's education. They say if you have one true friend you are the richest in the world, and luckily, I have many of them. I would like to thank my precious friends Elif, Erdi, Luca, Fra, Giammi, Valeria, Mete and Haktan who were my biggest supports in this journey.

Finally, I must express my very profound gratitude to my parents Ali and Dilek Çoban, my dear sister Burçe Çoban and to Mattia Gandolfi for their unwavering support and patience that cannot be underestimated. Good days ahead.

# Table of Contents

<b>List of Figures</b>	6
<b>List of Tables</b>	8
<b>Abbreviations</b>	10
<b>1. Introduction</b>	12
<b>1.1 Background and Problem Statement</b>	12
<b>1.2 Thesis Structure</b>	14
<b>1.3 European Commission Green Energy</b>	15
<b>1.4 Italian Territorial Context</b>	19
<b>1.5 Aosta Valley</b>	22
<b>2. Literature Review</b>	25
<b>2.1 The Factors and Data Sources</b>	25
<b>2.1.1 Physical potential</b>	26
<b>2.1.2 Geographical potential</b>	26
<b>2.1.3 Technical potential</b>	27
<b>2.1.4 Economical potential</b>	27
<b>2.2 Current Methodologies</b>	27
<b>2.3 Comparison of Different Methodologies</b>	33
<b>2.3.1 Top-down and Bottom-up approaches</b>	35
<b>2.3.2 Black-box, Grey-box and White-Box approaches</b>	36
<b>2.3.3 Input Data</b>	37
<b>2.3.4 Error Estimation</b>	38
<b>2.3.5 Error Band Estimation</b>	40
<b>2.4 Solar Photovoltaics</b>	42
<b>2.4.1 Solar PV Applications</b>	42
<b>2.4.2 Photovoltaic Cell Technologies</b>	43

<b>3. Methodology</b>	<b>44</b>
<b>3.1 Preliminary data collection and preparation</b>	<b>44</b>
3.1.1 Meteorological data	44
3.1.2 Territorial data	45
3.1.3 Slope	45
3.1.4 Aspect	46
3.1.5 Principle of Solar Radiation	46
3.1.6 Equinoxes and summer and winter Solstices	48
<b>3.2 Tools and Software</b>	<b>50</b>
3.2.1 QGIS	51
3.2.1.1 Description and functionality	51
3.2.1.2 WMS and WFS	51
3.2.1.3 DTM, DSM, and DEM	51
3.2.1.4 Graphical modeller	53
3.2.1.5. QGIS CRS	54
3.2.1.5.1. Working with Projections	54
3.2.1.5.2. Overview of Projection Support	54
3.2.2 UMEP	55
3.2.2.1 Solar Energy on Building Envelopes (SEBE)	57
3.2.2.2 Graphical modeller	60
<b>3.3 Shading Analysis</b>	<b>61</b>
3.3.1 Solar Radiation, Daily Shadow Pattern	61
<b>3.4 Combination of SEBE and Shading Analysis</b>	<b>63</b>
3.4.1 Graphical Modeller	67
<b>4. Results and Discussion</b>	<b>68</b>
<b>4.1 Photovoltaic potential assessment workflow</b>	<b>68</b>
4.1.1 Evaluation of the technical potential	70
4.1.2. Shading Analysis of Aosta	71
<b>4.2 SEBE and Shadow Analysis for Aosta DSM 2.0</b>	<b>73</b>
<b>4.3 SEBE and Shadow Analysis for Aosta DSM 0.5</b>	<b>85</b>
<b>4.4 Indirect method</b>	<b>91</b>

4.4.1 Coefficient for Reduction	91
4.4.2 Eligible area estimation for PV installation	92
4.5 Comparison of different resolutions and methods	93
5. Improvements and Future Work	96
Bibliography	97

## List of Figures

Figure 1 Energy consumption according to energy source.[7] .....	16
Figure 2 Climate-neutral EU27 by 2050 via greenhouse gas reduction [9] .....	17
Figure 3 Annualised mean investment in two distinct time periods, correspondingly 2011-2020, 2021-2030, and additional greenhouse gas reduction between 2021 and 2030, in billions of dollars [10].....	17
Figure 4 Portion of energy consumption maintained by renewable energy resources in Italy (Mtoe) .....	20
Figure 5 Portion of energy consumption maintained by renewable energy resources in Italy (%).....	20
Figure 6 PV plants concentration in Italy .....	21
Figure 7 Power production from ground and buildings .....	22
Figure 8 Hierarchical distribution of physical, geometric, technical, and economic potentials[14].....	25
Figure 9 Rooftop photovoltaic potential essential factors [16] .....	26
Figure 10 Study area vs annual generated electricity obtained from published articles .....	28

Figure 11 Relation between Top down/ Bottom up and Black/Gray/ White box approach .....	34
Figure 12 Top down vs Bottom up approaches [53] .....	35
Figure 13 Input data classification and the number of studies they took place.....	38
Figure 14 Decreasing trendline of error with respect to the years that studies were accomplished .....	41
Figure 15 Direct, diffuse and reflected solar radiation [] (Newport, 2021) .....	47
Figure 16 The orbit of the Earth relative to the Sun .....	48
Figure 17 Sun path at Northern Hemisphere .....	49
Figure 18 Continuous black line represents the DTM whilst the DSM is showed as dashed red line [60] .....	51
Figure 19 DSM and DTM comparison[60] .....	52
Figure 20 Digital Surface Model vs Digital Terrain Model.....	52
Figure 21 Building footprints of Aosta .....	53
Figure 22 CRS for Aosta Simulations .....	55
Figure 23 Processors of UMEP plugin classification[59] .....	56
Figure 24 Workflow of solar irradiance analysis on building envelopes using SEBE model with necessary geodata[59] .....	57
Figure 25 Solar Energy on Building Envelopes [59] .....	58
Figure 26 Graphical modeller of SEBE .....	60
Figure 27 Solar radiation, Daily shadow pattern Dialog box[65] .....	62
Figure 28 Shadow rasters for four selected days .....	64
Figure 29 Building footprints and masked vector.....	65
Figure 30 Suitable area polygon and SEBE application on the area .....	66
Figure 31 Graphical model of shadow analysis .....	67
Figure 32 PV technical potential estimation workflow.....	69
Figure 33 Shadow pattern for 4 days.....	71
Figure 34 Binary shadow rasters for 4 days in Aosta (2m).....	72
Figure 35 Combined shadow rasters for 4 days in Aosta and building footprints on the right (2m).....	72
Figure 36 Aosta Building footprint 2 metres DSM.....	73
Figure 37 Aosta simulations SEBE error .....	74
Figure 38 Tiled Aosta DSM.....	75
Figure 39 Slope and Aspect.....	76
Figure 40 Aspect results for Aosta 2 DSM.....	77
Figure 41 Slope results for Aosta 2 metres resolution .....	78
Figure 42 Intersection of aspect and slope for Aosta 2.....	78
Figure 43 Shadowing rasters for 4 days in 2021 .....	80
Figure 44 Crossed unique shadow raster (further on the left and zoom on the right)...	80
Figure 45 Vectorized unique shadow results of lit areas .....	81
Figure 46 Wall aspect and Wall height results for Aosta 2 .....	81
Figure 47 SEBE results for Aosta 2 .....	82

Figure 48 Final SEBE results for Aosta 2 .....	82
Figure 49 Final SEBE results in detail for Aosta 2.....	83
Figure 50 SEBE and Shadowing analysis comparison.....	84
Figure 51 SEBE and Shadowing analysis comparison in detail .....	84
Figure 52 Tiled Aosta DSM for 0.5 resolution .....	85
Figure 53 South aspect (between 135-225) maps.....	86
Figure 54 South Aspect with building footprints.....	86
Figure 55 Slope and aspect results for Aosta 0.5 DSM .....	87
Figure 56 Wall height and Wall aspect maps for Aosta 0.5 .....	87
Figure 57 SEBE results for Aosta 0.5 .....	88
Figure 58 SEBE results for Aosta 0.5 in detail.....	89
Figure 59 Shadowing analysis rasters for 4 days .....	89
Figure 60 Shadowing analysis result for Aosta 0.5 (Lit Areas) .....	89
Figure 61 Lit areas with Building footprint for Aosta 0.5 .....	90
Figure 62 Vectorized lit areas as result of shadowing analysis .....	90
Figure 63 SEBE and shadowing analysis comparison for Aosta 0.5.....	91

## List of Tables

Table 1 Growth targets and trajectories for 2030 for the renewables share in the electricity sector (TWh)	19
Table 2 Gross production of photovoltaic systems comparison between Aosta Valley and Italy	24
Table 3 Number and power of PV systems comparison between Aosta Valley and Italy	25
Table 4 Different methodologies throughout years and their comparison	35
Table 5 Black/Grey/ White box approaches	39
Table 6 Error estimation according to different studies held in literature review	41
Table 7 Error estimation/ Uncertainty/ confidence level	42



# Abbreviations

SDG	Sustainable Development Goals
WEO	World Energy Outlook
GHG	GreenHouse Gases
RES	Renewable Energy System
IoT	Internet of Things
QGIS	Quantum Geographic Information System
EU	European Union
GSE	Energy Services Manager
PAN	National Action Plan
DEM	Digital Elevation Model
DSM	Digital Surface Model
CDSM	Canopy Digital Surface Model
DTM	Digital Terrain Model
EP	Economic Potential
GG	Geographical Potential
GUI	Graphical user interface
NGEU	Next Generation European Union
PP	Physical Potential
PV	Photovoltaic
RES	Renewable Energy Sources

SEBE	Solar Energy on Building Envelopes
SEP	Spatial Energy Planning
TP	Technical Potential
UMEP	Urban Multiscale Environmental Predictor
WFS	Web Feature Services
WMS	Web Map Services
GSE	Energy Services Manager
EC	Energy Consumption
STC	Standard Test Condition
PR	Performance Ratio
CRS	Coordinate Reference System
WKT	Well Known Text
OTF	On The Fly

# Chapter 1

## 1. Introduction

### 1.1 Background and Problem Statement

Energy structure may be optimised and efficiency can be increased by exploring and using clean energy sources like solar energy. One of the most important ways that towns and communities may transition to lower carbon energy sources and behaviours is through solar energy and solar photovoltaic systems. If sustainability is to be taken seriously, large-scale solar PV installation must be taken into account, making the identification of possible acceptable roof space crucial for PV deployment modelling.

Throughout history, the climate of the Earth has been undergoing ongoing change. The average worldwide temperature today is more than  $0.85^{\circ}\text{C}$  warmer than it was during the final decades of the 19th century. In addition, the period from 1983 to 2012 was the warmest in the Northern Hemisphere in the previous 1400 years. [1] The deterioration of mountain glaciers and hotspots of biodiversity are just two of the significant effects this temperature rise is having on Earth. Anthropogenic forcings, such as the rise in Greenhouse Gas (GHG) concentrations, account for the majority of the factors promoting climate changes in the world average surface temperature. [2]. The combustion of fossil fuels and industrial activities, which accounted for 78% of all emissions beginning in 1970, are the sources of these anthropogenic GHG emissions. Production of electricity and heat accounts for 25% of this, followed by buildings (6.4%), agriculture, forestry,

and land use (24%), industry (21%), transportation (14%), industry (21%), other energy production (9.6%), and industry (24%).[1]

One of the key areas for achieving the Sustainable Development Goals (SDG) of the 2030 Agenda is energy. The United Nations Framework Convention on Climate Change's Paris Agreement objectives must be met in order for there to be a transition to sustainable energy production and solutions. [3] The energy sector is undergoing the most complicated upheaval since it was founded, with electricity becoming the "fuel" of choice as its proportion of global final consumption approaches 25% and is only going to increase. Rapid expansion is being fueled by political support and falling technology prices, but to secure a dependable, economical, and sustainable supply, the entire system must adapt and function differently. These are the three most crucial WEO keywords.[4]

Given the complexity of the issue statement and the difficulty of finding a comprehensive solution, it is recommended to combine different approaches to reach the optimal compromise. Three main elements are necessary for a safe and secure transition to cleaner renewable energy sources:

- Decreasing cost: As technology is used more and more, it grows, captures significant market share, and investments are repaid. Cost reduction is crucial because established technologies, such as hydroelectric and geothermal energy, have been competitive. However, even the most optimistic observers were shocked by the sharp decline in prices, as solar and wind energy can now outperform conventional generation technologies in many of the world's largest markets.
- Public opinion: It can also be a strong factor for change since consumers are choosing products and services with a more sustainable footprint, and social movements are pressuring governments to establish market incentive programs to encourage the switch from fossil fuels to RES and for businesses to cut back on carbon emissions and air pollution.
- Technological innovation: Higher solar photovoltaic module efficiencies and taller wind turbines have both contributed significantly to the development of renewable hydrogen produced through electrolysis. New frontiers are being opened by innovations; for instance, digital technologies like smart grids, the Internet of Things (IoT), big data, and artificial intelligence may assist to increase productivity and hasten the development of smart generation and distribution systems.

Comparing the outcomes of developing potential scenarios and doing a sensibility analysis of the models used that fulfil the aforementioned requirements is doable, but it necessitates documentation work as well as an easy means to deliver data and thorough information. Each scientific research and study has its advantages and disadvantages, but they frequently ignore elements that cannot be measured, such social and environmental dangers and opportunities, or they only cover a narrow range of potential changes.[5]

## **1.2 Thesis Structure**

The introduction chapter of this master's thesis provides background information and outlines the project's issue statement and presents a summary of Italy's current territorial and energy structure as well as a quick viewpoint on the case study that will be the subject of our next analysis. The next chapter, chapter 2, is devoted to a review of the literature using current methodologies. It includes a thorough investigation of each methodology, covering everything from the potentials that were examined and had a real impact on the research to the study's most interesting findings. This chapter will be very descriptive, but it will also be crucial because the key points will be fully covered. The main section of the thesis, Chapter 3, discusses the novel and adaptable methodology used to evaluate the technical potential of solar energy from photovoltaic sources. The first component of the master's thesis introduces the data collection, tools, and software. QGIS, the geographic information system, which is used in the methodology and is further discussed in the next subchapters, is the most crucial part of this section and for the entire master's thesis. The introduction of shading analysis for four seasons is the main topic of this chapter's final section. Using Aosta Valley as a case study, Chapter 4 applies the methodology and conducts a spatial analysis. The numerical findings are then presented and analysed. This chapter compares the results of two distinct raster resolutions and embodies various methodologies that have been applied to those two raster resolutions. Finally, the conclusions of the entire thesis are found in Chapter 5. In order to provide a more comprehensive understanding of the subject under study, the key findings are summarised together with ideas and suggestions for how the technique could be improved in the future.

### **1.3 European Commission Green Energy**

Since the production and consumption of energy account for more than 75% of greenhouse gas emissions, decarbonizing the EU's energy system is essential to meeting the 2030 climate goals as well as the long-term goals, such as carbon neutrality by 2050.

[6] Following are 3 essential tenets for the clean energy transition that will lower pollutant emissions and improve inhabitants' quality of life:

1. Ensuring a safe and reasonable energy supply for the EU
2. Creating a fully integrated, networked, and digital energy market in the EU
3. Prioritising energy efficiency, enhancing building energy performance, and creating a power sector that relies heavily on renewable energy sources.

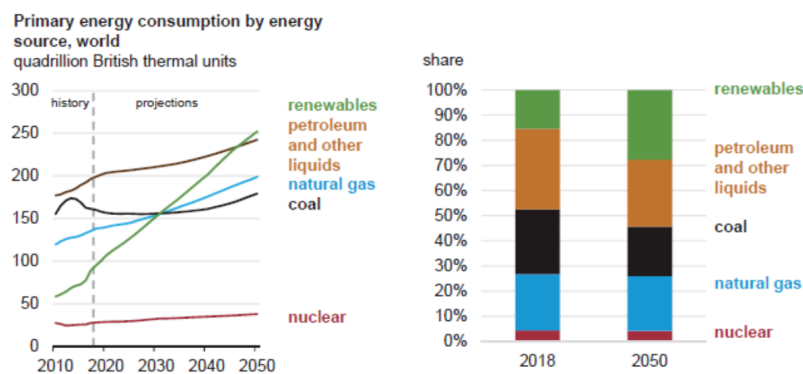


Figure 1 Energy consumption according to energy source.[7]

The Commission's primary goals are:

1. Developing more integrated grids and networked energy systems to support renewable energy sources.
2. Supporting cutting-edge infrastructure and cutting-edge technologies.
3. Improving product eco-design and energy efficiency.
4. Decarbonizing the gas industry and encouraging smart sector integration.
5. Giving customers more influence and aiding EU nations in combating energy poverty.
6. Encourage the global use of EU energy standards and technology.

In order to reduce net greenhouse gas emissions by at least 55% by 2030 compared to 1990 levels, the Commission adopted a series of suggestions. These proposals are mainly about making the EU's climate, energy, and transport cleaner and include taxation strategies. The major goal is to make Europe the first continent in the world to be climate neutral.[8]



Figure 2 Climate-neutral EU27 by 2050 via greenhouse gas reduction [9]

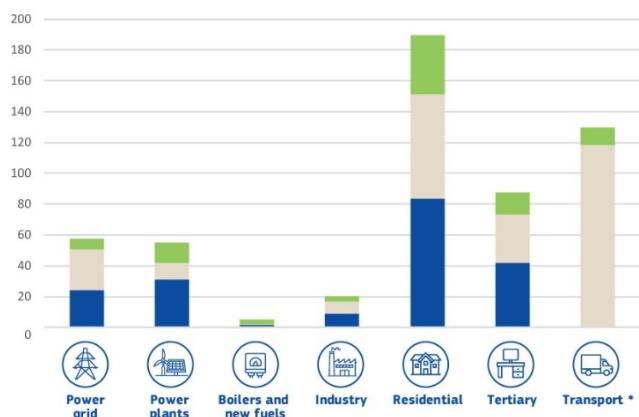


Figure 3 Annualised mean investment in two distinct time periods, correspondingly 2011-2020, 2021-2030, and additional greenhouse gas reduction between 2021 and 2030, in billions of dollars [10]

From 2011 through 2020, the energy system's historical annual investments are shown by the colour blue. Grey is used to highlight the additional 2030 policies that will be in place in 2021–2030 compared to the 2011–2020 timeframe. The additional greenhouse gas reduction needed to reach a -55% target between 2021 and 2030 is indicated by the green colour. [10]

*Table 1 Growth targets and trajectories for 2030 for the renewables share in the electricity sector (TWh)*

Year and annual trajectory	2016	2017	2025	2030
Renewable production	110.5	113.1	142.9	186.8
Hydropower	42.4	46.2	49.0	49.4
Wind	17.7	17.7	31.0	41.5
Geothermal	6.3	6.2	6.9	7.1
Bioenergy	19.4	19.3	16.0	15.7
Solar	22.1	24.4	40.1	73.1
Denominator- Gross inland consumption of electricity	325.0	331.8	334	339.5
RES-E share(%)	34.0%	34.1%	42.6%	55.0%

In conclusion, increased use of renewable energy directly lowers the negative consequences of fluctuating global fossil fuel prices and exchange rate concerns associated with energy spatial and logistic monopolies. The EU's dependence on fossil

fuel imports, vulnerability to global shocks, and price unpredictability will be reduced thanks to the recently agreed-upon aggressive 2030 renewable energy and energy efficiency targets. Innovation will be needed to achieve the sustainable transition, and this innovation will be stimulated by investments in renewable energy and energy efficiency. The EU will be able to comply with the Paris Agreement thanks to these investments.[2],[10]

## 1.4 Italian Territorial Context

In general, renewables growth in Italy has outpaced expectations while final consumption has decreased. As a result, in terms of percent, the EU Agenda has been fulfilled in advance in each of the three sectors:

- *Power sector* : 107.6 TWh in 2014 vs 79.0 expected (99 in 2020)

- The target % for the power sector is 26.4%. In 2014 Italy had already reached 33.4%, while the expected intermediate target was 21.7%.

- Renewable power targets will be revised from 26% to 32-35% (120-130 TWh)

- *Thermal sector*: 9.9 Mtoe (2014) vs 5.5 expected (10.5 in 2020)

- *Transportation sector*: 1.5 Mtoe(2014) vs 2.14 expected (3.45 in 2020)

The report provided by the GSE (Energy Services Manager), which is divided between the Electrical and Thermal sector and Transportation, is the source of many of the data presented below, which are the results of the collection of statistical data on the production of energy from renewable sources on the Italian territory. The purposes are both routine statistical production and the monitoring of energy consumption targets from RES established by Directive 2009/28/EC and the National Action Plan (PAN) for renewable energy. [11]

The graphs below display the amount of RES used in the electric sector from a gross power and percentage perspective, as well as taking the PAN trajectory of the prior strategy into account. Italy is doing well, performing even better than the dark blue line, indicating that we are exceeding our goals and that there is still room for improvement as more electricity from RES is being shared.[11]

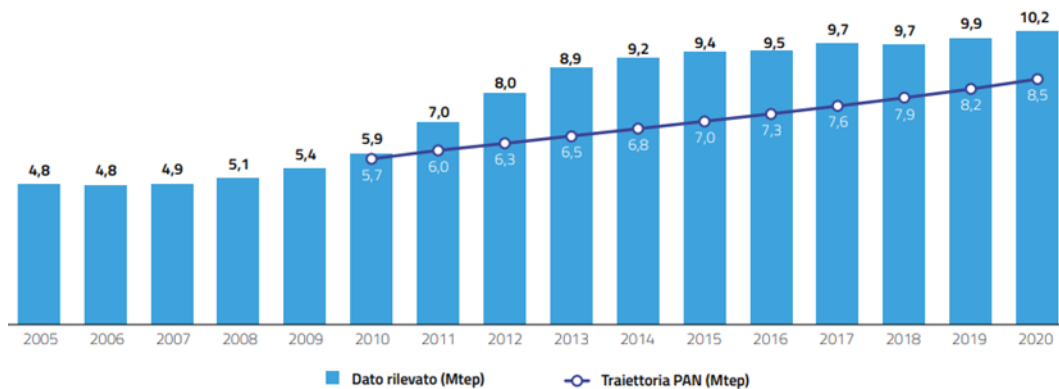


Figure 4 Portion of energy consumption maintained by renewable energy resources in Italy (Mtoe)

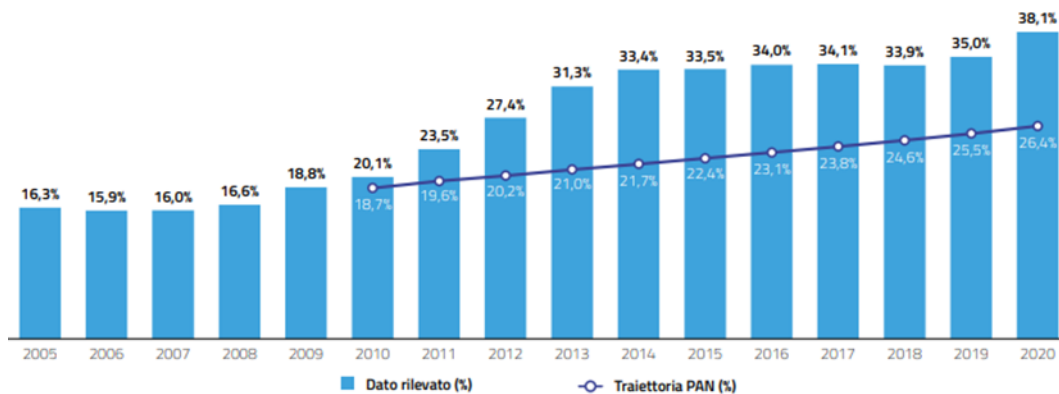


Figure 5 Portion of energy consumption maintained by renewable energy resources in Italy (%)

At the end of 2020, there were just under 949,000 installed renewable energy power plants in Italy, the majority of which are solar systems (98.6% of the total), which have expanded by about 56,000 units since 2019 (+6.0%). With an increase of roughly 1,091 MW over 2019 (+ 2.0%), the gross efficient power of installed plants is equal to 56,586 MW. This trend is primarily driven by the growth dynamics seen in the solar (+785 MW) and wind (+192 MW) sectors.[12]

The 935,838 photovoltaic systems installed in Italy as of 31 December 2020 correspond to a power equal to 21,650 MW. In the solar year 2020 alone, just over 58,000 systems were installed, for an installed capacity total of 749 MW<sup>2</sup>; 27% have a power lower than or equal to 3 kW, 68% between 3 kW and 20 kW, the remaining 4% greater than 20 kW. Compared to 2019, the plants that entered into operation in the calendar year decreased by 4.5%; the variation of the installed power, on the other hand, is negligible.



Regarding the quantity of solar systems built in Italy, 35% of the installed power is concentrated in plants with a size between 200 kW and 1 MW, while 92% of the plants have a power of less than 20 kW. The total power generated by photovoltaic systems accounts for 38% of the total power generated by the national park of renewable energy sources.

The graph below explains the various installation typologies by differentiating between those that are installed on the ground and those that are mounted primarily on other buildings, such as rooftops.

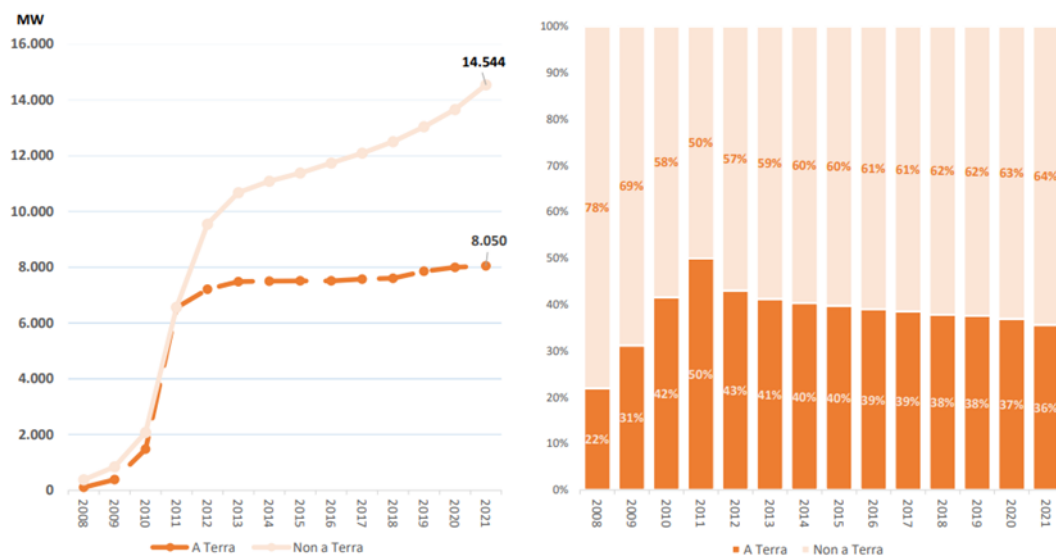


Figure 7 Power production from ground and buildings

## 1.5 Aosta Valley

After reading the study held in the previous subchapter, it should be evident why we chose to concentrate our attention on the city of Aosta, which is situated in the midst of the Aosta Valley, a valley that is entirely encircled by mountains.

Aosta has a more continental climate than one that leans toward the alpine from a climatic perspective. On the other hand, summers are brief but nonetheless exceedingly hot. When it comes to lowest temperatures, especially in February, temperatures tend to

drop very abruptly and frequently stay below zero. However, in full daytime, especially toward the end of the month, surroundings can easily reach 12 to 13 °C.

The highest daytime temperatures, particularly in the presence of strong sun with African anticyclone, surged rapidly upward, stalling in the basin and reaching 25–26 °C. The monthly record for February dates back to 2017, when it hit 19 °C on February 27. The peak of heat, precipitation, and heat storms all occur in the months of June and July. The only months with mild morning temperatures, around 15 °C, and extremely high maximum temperatures, with peaks typically around 32 °C or 33 °C but with the most intense heat waves reaching up to 35 °C, are June and July. The capital of Aosta hit 40 °C on June 27, 2019, setting an absolute record for heat. The last thunderstorms are seen around the end of August, when temperatures suddenly plummet. In September, normal values and daily maximum values in the morning are 30 °C. In October, the climate significantly cools down with the first values below zero in the middle of the month and the maximum diurnal values struggling to achieve 20 °C. Snowfalls are severe and regular in November and December, when minimum temperatures are frequently below zero.

This meteorological overview was written to make it clear that, although being in northeastern Italy, the area is, on occasion, very sunny and that there are rigorous regulations to follow in order to maximise solar energy generation and sharing.

The following data demonstrate the poor energy output and low number of installed PV plants in Aosta City, which is why it is at the bottom of the Italian ranking by region. Additionally, the difference between 2020 and 2021 is not encouraging for technical advancement.[13]

*Table 2 Gross production of photovoltaic systems comparison between Aosta Valley and Italy*

	<b>Production (GWh)</b>		<b>Incidence on the national total (%)</b>		<b>Variation % of the production</b>
	<b>2020</b>	<b>2021</b>	<b>2020</b>	<b>2021</b>	<b>2021/2020</b>
<b>Aosta Valley</b>	<b>27,8</b>	<b>27,9</b>	<b>0,1</b>	<b>0,1</b>	<b>0,3</b>
<b>Italy</b>	<b>24.941,5</b>	<b>25.039,0</b>	<b>100,0</b>	<b>100,0</b>	<b>0,4</b>

Table 3 Number and power of PV systems comparison between Aosta Valley and Italy

	2020				2021				% 21 / 20	
	n°	%	MW	%	n°	%	MW	%	n°	MW
Aosta Valley	2.592	0,3	25,4	0,1	2.759	0,3	26,4	0,1	6,4	4,1
Italy	935.838	100,0	21.650,0	100,0	1.016.083	100,0	22.594,3	100,0	8,6	4,4

We were able to learn more about the energy situation in Aosta and how to improve it with the aid of the Energy Center, a research centre affiliated with the Polytechnic in Turin that is based on the themes of energy, sustainability, and innovation. The Energy Centre's mission is to launch a number of actions and projects that will offer support and strategic advice to local authorities, national, and transnational bodies, on energy policies and technologies to be adopted.

# Chapter 2

## 2. Literature Review

The next chapter analyzes the literature theory of this thesis in brief, going over the different methodologies available to determine the potential of rooftop solar energy systems in various areas and identifying the best ones to enhance the ones now in use for future studies. This chapter is divided into the following three sections: 2.1 introduces numerous influencing elements and common approaches for examining our key research factors, such as physical, geographic, technological, and economic potential. In sections 2.2 and 2.3, various approaches for observing the rooftop PV potential are investigated, and information on these methodologies is shown in order to improve future work prospects.

### 2.1 The Factors and Data Sources

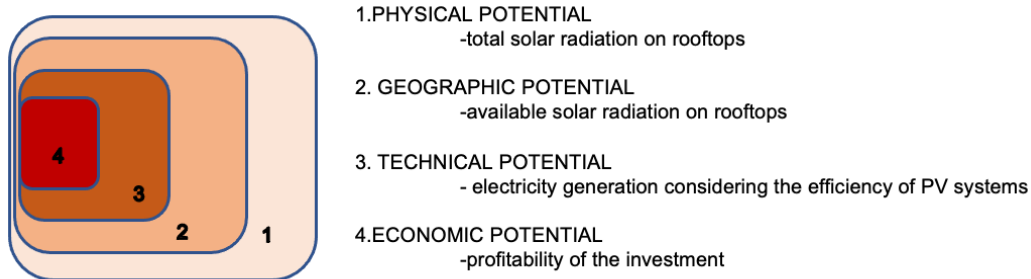


*Figure 8 Hierarchical distribution of physical, geometric, technical, and economic potentials[14]*

A hierarchical methodology is considered as the most reasonable means of evaluating the potential of renewable energies.[15]

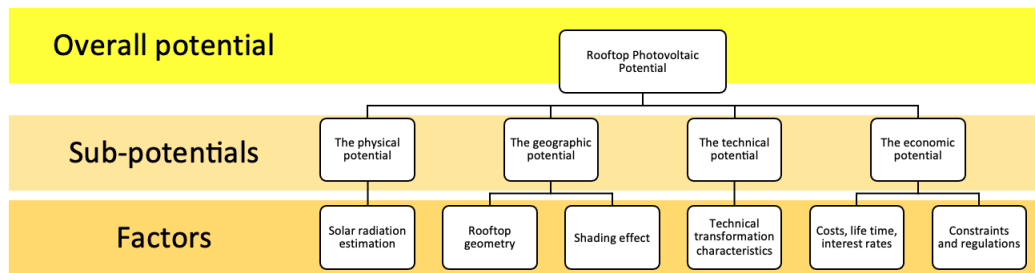


Figure 9 Rooftop photovoltaic potential essential factors [16]

As a result, it is clear that the schematic hierarchical categorization of our influencing elements is very typical and well shared throughout the numerous scientific articles that have been analysed. The idea behind developing the methodology is the same for each of them, regardless of whether they are plotted as circles inside of each other or more parallelly.

### 2.1.1 Physical potential

The amount of solar energy that is radiated onto the earth's surface annually can be referred to as physical potential. Due to the earth's rotation and the longitude and latitude coordinates, the radiative flux incident at a particular site depends on the time of day and year. Due to reflection, scattering, and absorption of radiation in the atmosphere, the radiative flux is decreased as it travels through the atmosphere and reaches the surface. Albedo refers to the percentage of incoming radiation that is reflected back into space by the earth's atmosphere.[15]

It is an indication of the resource's maximal energy capacity. This potential can be assessed in a variety of ways depending on the different uses.[17] It is determined as the horizontal irradiation in Izquierdo's article, which is computed using the following log-standing procedures: Making monthly irradiation maps, calculating the monthly clearness index for the locations with hourly meteorological data, computing the monthly extraterrestrial radiation, which is rooted in the geometry of the sun-earth system, and examining the impact of hourly shadows on monthly values considered with geometrical calculations with digital terrain model.[18]

### 2.1.2 Geographical potential

Geographical potential is evaluated in terms of the impact of the built environment and geographic constraints. By removing restricted areas like highways, beaches, lakes, and rivers as well as safeguarded regions like national parks, the spatial potential of

renewable resources can be realized.[19] The appropriate portion of theoretical potential that is usable because the area or location is acceptable and easily accessible. Only roof surfaces suitable for solar installations will be included in the geographic potential since only photovoltaic plants on roofs are taken into account.[20]

### **2.1.3 Technical potential**

Technical potential is the quantity of energy that, under certain conditions and conditions of time and place, is exploitable. The technical potential can alternatively be conveniently defined as an irradiation that is technically usable while also taking into account the effectiveness of photovoltaic modules.[20] The amount of energy produced by photovoltaic panels erected on building roofs in the available area in Aosta Valley, Piedmont, Italy, while taking into account shading effects, is the technical potential in this scenario.

### **2.1.4 Economical potential**

The fraction of technological potential that can be used commercially is known as economic potential. It accounts for expenses and socioeconomic elements including the cost of fuel and electricity, lost opportunities, and land prices. The amount of electricity generated by the rooftop solar PV system should be determined after choosing the system size and business strategy. Later, it will be possible to determine the rooftop solar PV system's profitability and, ultimately, its economic potential.[21] Economic and Implementation Potentials will not be covered in this thesis.

## **2.2 Current Methodologies**

This chapter's goal is to analyse each paper in detail in order to fully describe our literal review. It will be lengthy and verbose, but this is the only way to fully comprehend which methodologies have been studied thus far and which ones might benefit from further research and development in order to determine the true purpose of this thesis project. A very fascinating graph is shown below, which compares the annual output of power in that specific area to the width of the researched area extension, which is typically

referred to as the geo-scale which will be explained in more depth in following chapters. The goal is to demonstrate that this correlation exhibits a consistent pattern across all papers, but that there isn't really a proportionality affecting the two variables. In reality, there are many variables that affect the calculation of solar potential, including the suitability of the rooftop area geographically and the solar irradiance on the ground which can be referred to as physical potential. Our goal is to determine why this occurs and how to improve the process to get the most accurate, scalable results possible.

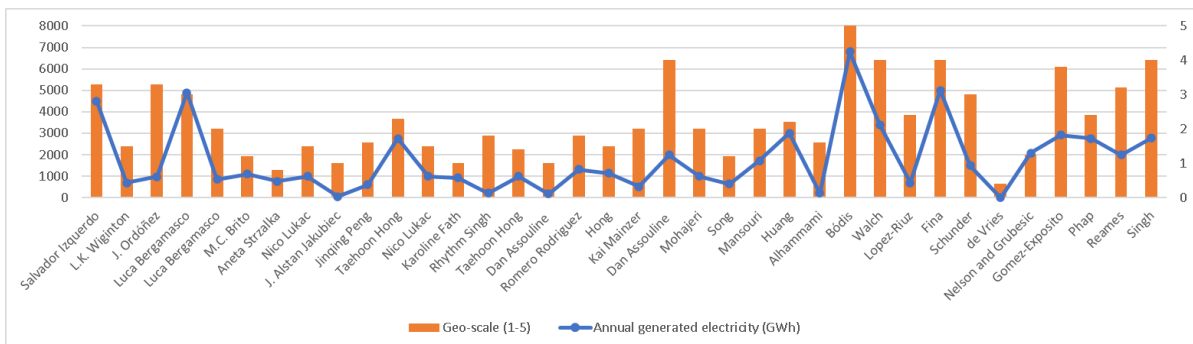


Figure 10 Study area vs annual generated electricity obtained from published articles

The 36 scientific papers are ordered by year of publication:

1. In order to determine the technological potential of rooftop solar systems, urban regions of Spain were examined in April 2008 using a bottom-up methodology. Based on statistically representative GIS vector maps of land uses and building density, research was conducted. To determine the energy capacity of photovoltaics on rooftops, statistical construction data and Google Earth digital metropolitan maps that are generated and scaled with AutoCAD are utilised. The building type, location, shading impact, tilt angle of the roof, and orientation were all potential sources of inaccuracy that were taken into account by the correction factor. [18]

2. Residential structures in Andalusia, Spain were analysed using a top-down strategy that was based on statistical sampling in January 2010. Inputs for scaling in AutoCAD were urban satellite maps that were downloaded from Google Earth and statistical data. ([22]

3. In order to get roof areas, the "Feature Analysis" extraction tool in ArcGIS was utilised in January 2010 to evaluate the rooftop solar photovoltaic potential of residential structures in Ontario, Canada. Later, shading and orientation were taken into account to improve accuracy. Finally, an economic assessment was carried out using market pricing.[23]

4. The Piedmont region was used as a case study in February 2011 to determine the photovoltaic solar potential using a hierarchical framework. A geographic cadastral study was conducted using numerical technical regional maps. ArcGIS and MATLAB were used to process and analyse the maps. Shadowing impact was taken into account.[24]

5. On the basis of ortho image analysis, a city level top down approach was taken into consideration for the study in September 2011. The analysis, which was carried out in Matlab using aerial photography, 3D models, and satellite maps, is a more thorough assessment of a prior scientific publication by the same authors.[25]

6. LiDAR data was used to construct DTM and DSM, population distribution, and solar radiation modelling by the ArcGIS solar analyst extension tool in November 2011 to estimate the photovoltaic potential in Lisbon, Portugal. [26]

7. Stuttgart family homes' rooftop solar potential was calculated in January 2012 using a bottom-up approach consisting of extraction algorithms on PV system simulations. The approach took as inputs 3D models, LiDAR data, and geoinformation systems. [27]

8. To determine the solar potential and sustainability of photovoltaic system installation in Maribor, a bottom-up methodology using LiDAR data, pyranometer measurements of solar irradiances, a Heuristic vegetation shadowing model, and multi-resolution shadowing model was developed in September 2012. [28]

9. In May 2013, a bottom-up approach was used to determine the rooftop PV potential for hotels and other commercial buildings in Hong Kong. As inputs, LiDAR and statistical data were employed. [29]

10. In May 2013, a bottom-up approach was developed in Cambridge, USA, combining a combination of 3D models, GIS, and LiDAR with Dayism irradiation simulation engine, rooftop temperature, and meteorological climate data, to predict the photovoltaic potential for a city-level geographical area. Online mapping and financial modules can be used with the outcome to pique building owners' interest in placing solar panels on their structures.[30]

11. South Korean photovoltaic systems' electricity generation was estimated using a bottom-up approach at the city level in March 2015. The method also included a sensitivity study of the effect parameters, and the outcomes varied depending on the slope, azimuth, and geographical characteristics. The inputs used were statistics data and satellite maps.[31]

12. A bottom-up approach to estimating nonlinear photovoltaic potential was put forth in Maribor in March 2015. The case study results were produced by comparing the constant and nonlinear efficiency characteristics of solar photovoltaic inverters and photovoltaic module types, and this method incorporated the impacts of topography, vegetation, and shadowing that are critical for the accuracy of the case study. As inputs, LiDAR and 3D models were employed.[32]

13. Mumbai's (India) photovoltaic potential was assessed in June 2016 utilising a top-down process that included GIS image analysis, high-granularity land public data, and PVSyst sunshine simulation. The PVSyst's mathematical models and micro-level simulations used the same methods. As inputs, satellite maps, statistical data, and aerial photography were all employed.[33]

14. In November 2016, a top-down strategy was used in urban areas, taking facades into account. The investigation included LiDAR, 3D models, and statistical information.[34]

15. After noticing the strong influence of shadowing elements, a bottom-up methodology was created in April 2017 to determine South Korea's physical and technical potential. The technique was developed employing hillshade analysis, and its primary goal was to examine building shadowing. The analysis was completed using statistical data and satellite imagery.[21]

16. In May 2017, a bottom-up approach based on support vector machines was used for urban areas within communes (SVM). As inputs, LiDAR data, 3D models, and aerial photos were all incorporated.[35]

17. In September 2017, a top-down methodology for calculating the regional and metropolitan scale of Ludwigsburg's photovoltaic potential using CityGML geography descriptions and 3D models for simulations, analysis, and visualisation on the SimStadt platform was employed. As inputs, 3D models and statistical data were used.[18]

18. A large district level bottom-up approach was implemented in June 2018 using the ArcGIS Hillshade tool. As inputs, 3D models and statistical data were used.[36]

19. A city-level top-down approach based on machine learning and image recognition was conducted in July 2017. The inputs taken into consideration were satellite, statistical, and aerial photography.[20]

20. In September 2017, a bottom-up strategy using a random forest model at the national level was taken into consideration for the study. The methodology can be summed up as follows: gather data on variables, train a random forest model using the data, and use the model to predict variables at unidentified places. Data inputs included high-resolution aerial images and statistical information.[37]

21. A city level bottom up method was taken into account in the research in June 2018 and included feature selection, dataset scaling, data labelling, support vector machine (SVM) testing, and training. As inputs for the analysis, LiDAR, a 3D model, and statistical data were collected.[38]

22. The complex topography of a city-level geographic area was modelled as a digital elevation model in November 2018 using remote sensing data. The roof segment file was afterwards constructed using a bottom-up approach, and it was ran through a dissolve function to combine adjacent polygons with a particular attribute to make continuous acceptable sections. The rooftop polygon file was then categorised and converted to a raster file.[39]

23 In order to calculate the solar PV potential at a small town level, simulation of the monthly and annual solar radiation on rooftops at an hourly time step was carried out in November 2018. This bottom-up strategy is focused on the extraction of rooftop features from remote sensing photos. High-resolution remote sensing picture data were used to recover 2D rooftop outlines and 3D rooftop characteristics. [40]

24. The PV potential was calculated in April 2019 using a bottom-up approach at the city level. The total area of building roofs that are usable must first be determined. Next, the annual radiation available per unit area, which is based on the area discovered in the first step and the weather conditions, must be determined. Finally, the U-Net deep learning method was used, using 3D models and satellite images as inputs.[41]

25. A bottom-up strategy was used in June 2019 on a city-level geographic area. Esri ArcGIS software was used to calculate the number of buildings, their types, and their rooftop areas in order to assess the economic performance and rooftop solar system energy potential of Khalifa and Zayed (Abu Dhabi). [42]

26. A continent level top down strategy was taken into consideration for the research in July 2019. In order to offer an accurate assessment of the technological potential for rooftop PV power production with a geographical resolution of 100m across the European Union, the methodology combines satellite-based, statistical, and machine learning data sources.[43]

27. In order to handle huge spatio-temporal information, a national-level bottom up method that combined machine learning, GIS processing, and physical models was taken into consideration for the research in December 2019. Additionally, standard deviations were used to quantify the uncertainties based on the statistical distribution of the variables included in the potential estimation. The investigation made use of LiDAR, 3D models, and statistical information.[19]

28. A city level top down approach that converts the amount of nighttime light intensity recorded by satellite radiometry into electricity usage was taken into consideration for the study in March 2020. At the conclusion of the procedure, the average electricity usage per family in various clusters was determined.[44]

29. To estimate a cost-optimal large-scale economic potential, a top-down strategy at the national level was used in June 2020. The analysis made use of statistical data.[45]

30. In July 2020, the residential rooftop solar potential in Erie County, USA, was discovered using remote sensing, LiDAR, footprint, and Google's Project Sunroof data. Digital Terrain Model, Digital Surface Model, and normalised Digital Surface Model were all created using LiDAR data. The project's outcome is that low-income people have comparatively little access to rooftop solar.[46]

31. The Quick-scan method was employed to calculate Eindhoven's solar potential in September 2020. The methodology entails creating a fitting algorithm for photovoltaic modules on rooftops and recreating virtual 3D roof parts. Aerial photography, weather, GIS, and LiDAR data are all cited as input data that were used for the case study. Solar Monkey, a photovoltaic GIS, as well as photovoltaic materials and devices, were used to determine the annual rooftop potential. The potential for rooftop solar energy was compared between UAS and LiDAR data. The rooftop solar radiation was calculated using the ArcGIS solar analysis tools.[47]

32. Rooftop photovoltaics' technical potential contribution to Spain's future electricity mix was examined in October 2020 using data from ArcGIS and the national geographic database. Five sustainable scenarios were examined, each with a different share of centralized renewables, rooftop PV, and storage.[48]

33. One-fourth of the city was taken into account as a geographical region in October 2020 for this research, which employed a bottom-up technique. Through the use of incredibly high-resolution UAS data, a digital elevation model was produced. In order to finally produce a workable and ideal roof extraction and energy calculation, edge detection and object delineation were carried out.[49]

34. Four distinct American cities were taken into account as a geographical area for the investigation in November 2020. Rooftop solar potential was estimated using a bottom-up methodology that included national statistics. the distribution of rooftop solar



The model that is used case by case to the various 36 scientific publications is the second intriguing aspect that has the biggest impact on our findings. In order to categorise them more precisely, we chose to group them according to whether they utilise a top-down or bottom-up approach: they are information processing and knowledge management techniques used to analyse problematic circumstances and provide suitable hypotheses for the necessary solution.

The black, grey, or white box is the third factor to be examined. In this instance, our goal is to categorise our literal review based on the amount of knowledge that is readily available and the ease of access to the data present in each individual scientific research. This method makes it possible to comprehend the potential degree of data sharing, the limitations, and the methodology utilised to create the rules that lead to the resolution of the issue in order to comprehend the effectiveness of open development.

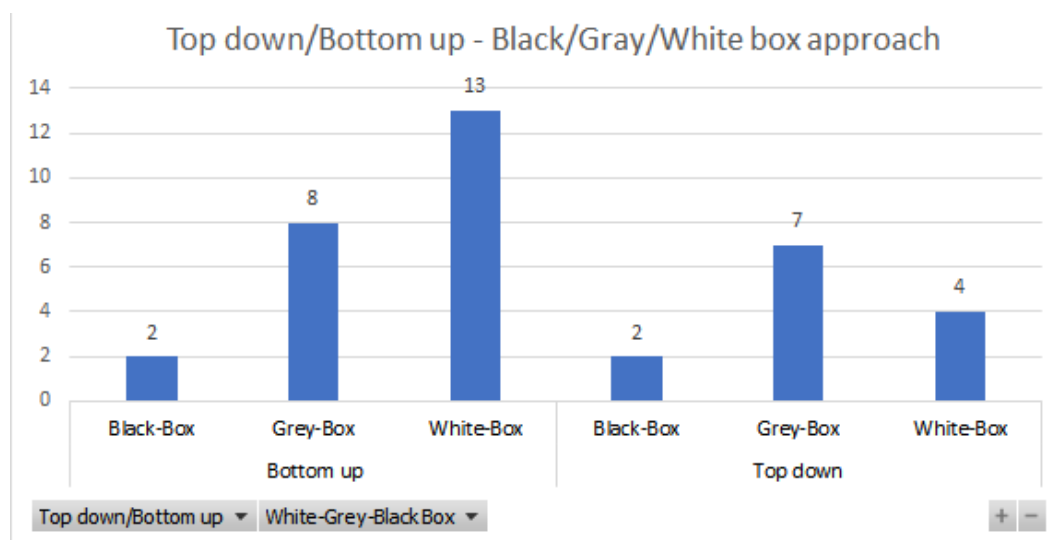


Figure 11 Relation between Top down/ Bottom up and Black/Gray/ White box approach

In the end, we sought to normalise our categorization from a more quantitative perspective, which is why a technique error band was developed. By offering a confidence interval on the calibre of the analysis, we attempted to decipher from each publication the reasons why there were uncertainties impacting the correctness of the results and the dependability of the methodology and tools mentioned. Nearly all of them revealed errors, primarily between the suggested technique of analysis and actual appraisals made using readily accessible physical tools on the market.

These interesting factors are analysed in more detail in the following subchapter.

### 2.3.1 Top-down and Bottom-up approaches

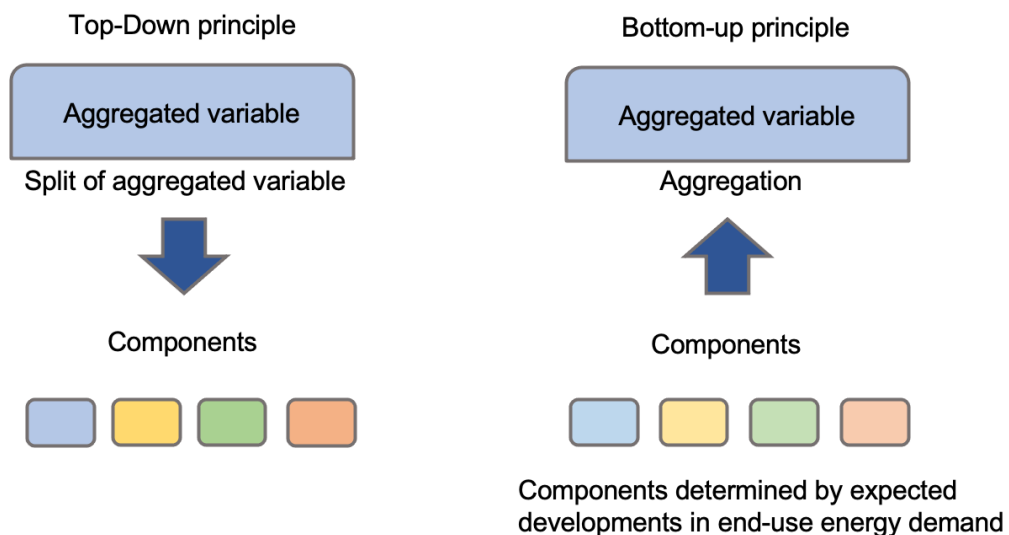


Figure 12 Top down vs Bottom up approaches [53]

The fundamental distinction between top-down and bottom-up techniques may be explained by looking at which way they move. The bottom-up technique begins with particular variables and ends with the general, whereas the top-down approach moves from the general to the specific. This causes the project sizes of the two methodologies to vary. [53] Since the bottom-up strategy is more tightly focused while the top-down strategy encompasses a larger region. In other words, the bottom-up method concentrates on specialised analyses locally and individually and integrates them all to create a global outcome, whereas the top-down method seeks the overall picture with all factors incorporated.

The traces of these two techniques have been found in the papers that were the subject of the literature review, and each article has been allocated to one of them as indicated in the table above. The majority of the present approaches can be shown to have a bottom-up approach (13/36). Since those studies primarily concentrated on a few particular elements, they investigated the technological potential of rooftops and later used the methodology in a large number of locations. Examples of these particular elements are shadowing factor and rooftop segmentation, and these studies are conducted in confined spaces with few structures. On the other hand, research that concentrated on bigger areas has adopted a top-down method.

### **2.3.2 Black-box, Grey-box and White-Box approaches**

Geospatial data refers to information that is stored along with a geographic indication of some type. The two basic categories of spatial data are vector data and raster data. Vector data refers to information that is represented by points, lines, and polygons, such as buildings, towns, roads, mountains, and water bodies. For example, a visual representation using vector data may display houses as points, roads as lines, and entire towns as polygons. Pixelated or gridded cells that are categorised by row and column make up raster data. These geographical data are employed in study as inputs, and as an output, the solar potentials were attained. Raster data pictures are substantially more complex and contain photographs and satellite images.[72]

The black-box technique is a method that informs the user and the analyst of input and result without providing any further details about the procedure, methodology, or computations involved in the analysis. The black-box method includes methodologies that use neural network functioning.[72]

The white-box approach, which includes comprehensive information regarding the internal logic and structure of the technique, is also known as the glass box, open box, or transparent box approach. The analyst should be well knowledgeable of the procedure. The majority of the statistical methods examined throughout the literature research are grouped under the heading "white box approach." [73]

A grey-box method combines both white-box and black-box thinking. A basic understanding of the procedure as well as some knowledge of the internal workings of

the analysis are all that are needed for this method. Black-box techniques are categorised as the majority of papers created only with QGIS.[72]

*Table 5 Black/Grey/ White box approaches*

No	Black Box	Grey Box	White Box
1	Fundamental aspects	Partial knowledge of internal working	Full knowledge of internal working
2	Low granularity	Medium granularity	High granularity
3	User acceptance	User acceptance	Developers and testers
4	External exceptions	High level database diagrams and internal states	Internals are fully known
5	Least time consuming	Average	Most time consuming
6	By trial and error	Data domains and internal boundaries can be tested	Test better data domains and internal boundaries
7	Not suited for algorithm testing	Not suited for algorithm testing	Suited for algorithm testing

### 2.3.3 Input Data

It was discovered that five distinct types of input data—airial pictures, LiDAR, 3D models, satellite maps, and statistical data—were used in the articles examined and summarised in chapter 3.2. This section goes into detail about these inputs.

- **Statistical Data**

The primary method used in the research was the use of statistical data, particularly census data, which includes information on the population, the economy, and the targeted research region. Basic demographic variables such as age, sex, marital status, household size, and composition are included in census statistics.[70] In addition to statistical census data, a significant number of studies also employed LiDAR data.

- **LiDAR data**

High resolution rasters of ground elevation with fine vertical precision are available in Light Detection and Ranging (LiDAR) data. The following equipment must be put on an aeroplane as part of the technology to be obtained: a laser scanner to transmit light pulses to the ground surface, a global positioning system (GPS), and an inertial navigation system (INS).[54]

- **3D Model**

The third sort of input is 3D model data, which is gathered from hundreds of photographs of intersecting aerial images taken by an onboard camera. These data are primarily used to create a 3D map of the region of interest in order to better see and analyse the building features. They do not differ from LiDAR data in that they do not contain elevation data.[61]

- **Satellite and Aerial data**

The other sorts of data used in modern techniques include satellite and aerial data. In comparison to aerial photographs, satellite photos are more expansive yet contain less detail overall.[61]

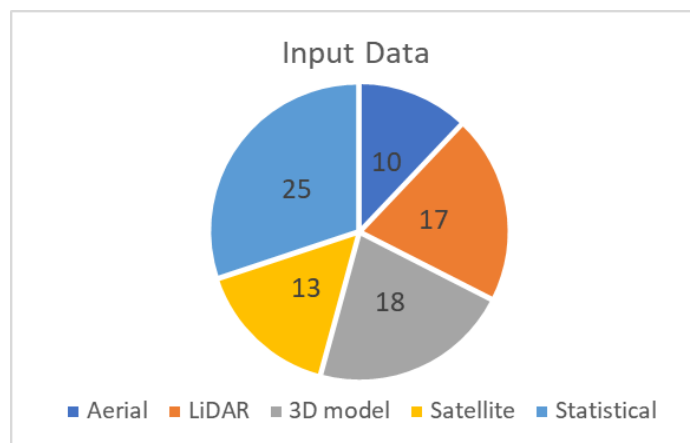


*Figure 13 Input data classification and the number of studies they took place*

### **2.3.4 Error Estimation**

The capacity to comprehend the precision of the estimation for the inaccuracy connected to the approach that is employed in every single article is the analysis's most intriguing outcome. We concentrated on the so-called absolute and relative uncertainty since it is a useful way to categorise the dependability and friendliness of the ratings.

Table 6 Error estimation according to different studies held in literature review

Classification				Error estimation								
#	Author	Geographic area	Geo-scale	Error (%)	Uncertainty	Uncertainty	Roof	Shading	Solar	Number	Method	Year
36	Salvador Izquierdo	Buildings within	3.3	13.00	32.00%	4.160	+				+	2008/04
35	J. Ordóñez	Residential	3.3	10.00	2.53%	0.253	+					2010/01
34	L. K. Wqinton	Residential	1.5	15.00	60.00%	9.000					+	2010/01
33	Luca Bergamasco	Piedmont Region	3	1.70	110.63%	1.881		+				2011/02
32	Luca Bergamasco	The whole city of	2	10.00	18.81%	1.881					+	2011/09
31	M.C. Brito	Urban region	1.2	20.00	9.40%	1.881	+	+	+		+	2011/11
30	Aneta Strzalka	Multi-family	0.8	25.00	7.52%	1.881	+	+				2012/01
29	Nico Lukac	Urban area-city	1.5	2.60	72.33%	1.881			+			2012/09
27	J. Alistan Jakubiec	City level	1	4.45	40.88%	1.819			+			2013/05
28	Jingqin Peng	Hotel and	1.6	12.50	15.05%	1.881			+			2013/05
26	Taeheon Hong	City level(due to	2.3	24.30	7.74%	1.881			+			2013/12
25	Nico Lukac	Large urban	1.5	12.00	19.63%	2.356					+	2014/01
23	Karoline Fath	Urban areas	1	15.00	12.54%	1.881		+	+			2015/03
24	Rhythm Singh	Buildings within	1.8	13.95	39.07%	5.450				+		2015/03
21	Dan Assouline	Urban areas	1	7.50	26.00%	1.950					+	2016/11
20	Romero Rodriguez	Federal State	1.8	13.00	14.47%	1.881			+			2017/04
19	Hong	Big district	1.5	15.00	12.54%	1.881			+			2017/05
18	Kai Mainzer	City level	2	10.00	30.00%	3.000	+	+				2017/07
17	Dan Assouline	Country scale	4	17.12	19.58%	3.352					+	2017/09
16	Mohaeri	City	2	13.00	34.00%	4.420					+	2018/06
14	Song	Small town	1.2	8.00	13.00%	1.040	+					2018/11
15	Mansouri	City	2	9.63	67.11%	6.466			+			2018/11
13	Huang	City	2.2	9.50	2.97%	0.282	+	+				2019/04
12	Alhamami	City	1.6	7.00	26.87%	1.881			+	+		2019/06
11	Bódis	European Union	5	15.00	1.80%	0.270					+	2019/07
10	Walch	Country	4	17.00	23.00%	3.910			+			2019/12
9	Lopez-Riu	Capital city	2.4	13.00	3.48%	0.452						2020/03
8	Fina	Country	4	13.00	14.47%	1.881				+	+	2020/06
7	Schunder	City	3	9.38	20.06%	1.881					+	2020/07
6	de Vries	Several buildings	0.4	7.00	8.00%	0.560	+	+				2020/09
5	Gomez-Exposito	Andalucía, Pais V	3.8	1.00	188.07%	1.881					+	2020/10
4	Nelson and Grubestic	North part of the	1.25	15.76	40.93%	6.450					+	2020/10
2	Phap	Capital city (30	2.4	20.00	0.73%	0.145			+		+	2020/11
3	Reames	4 metropolies	3.2	7.00	4.29%	0.300					+	2020/11
1	Singh	13 cities, 79M	4	4.54	0.24%	0.011					+	2020/12

In order to provide a quantitative assessment of our review while treating it as a milestone, we may determine the average value of the error estimation and its associated uncertainty at the very conclusion of the preliminary evaluation.

It should be noted that just the two red-highlighted uncertainty values dominate the error estimation. They are over 100%, as can be shown, which should be physically impossible or a sign of a measurement estimation error. Because of this, they come out as rather peculiar and can be disregarded. There are several statistical techniques for determining whether a datum should be regarded as an anomalous value rather than just a dubious value in relation to others. The chance of extracting the observations from the normal distribution that are farthest from the mean may then be calculated, and if they fall outside of the acceptable range, they can be disregarded.

We also made the decision to assign a numerical value to the standard deviation, a statistical dispersion index that is used to estimate the variability of our data population around a position index. In this case, the position index is the arithmetic mean of the error over the 36 scientific papers, so the standard deviation is measured in the same way as the observed values.

Table 7 Error estimation/ Uncertainty/ confidence level

Error Estimation			
Average Value	11,77	Uncertainty	1,88
Standard Deviation	5,76	Confidence Level	90-95%
Final Result (abs.)	11,77 ± 1,88		
Final Result (rel.)	11,77 ± 16,0%		

In statistics, identifying a single value for a parameter is sometimes insufficient; it is usually advised to provide the estimate along with an interval of likely values for the parameter, known as a confidence interval. [71] The latter is an interval that subtly describes the amplitude of the value associated with in terms of probability. It's visually equal to the region that the random variable's probability distribution curve occupies inside the interval under consideration, and in our situation, this value which is between 90 and 95 percent for each examined scientific paper is one we can rely on.

### 2.3.5 Error Band Estimation

We chose to plot the outcome results in order to better comprehend the actual state of development with reference to the methodology employed in our literature review, taking into consideration the previous description of the methods we used to analyse the estimation of the inaccuracy. In order to better visualise the trend line of the error band estimation, as can be seen on the x-axis, we choose to follow the chronological sequence of the papers' published dates.

Our data are statistically correlated in a useful way using a linear error regression. From the graph, we can see and understand that the uncertainty around the correctness of the estimates based on each individual approach is reducing with time. This is a significant result because it shows that solar potential estimation quality is improving with time, allowing us to base our knowledge on ever-more accurate mathematical and logical projections.

In order to address the issue with other closed tools, like ArcGIS and MATLAB, which restrict access to the potential concept of open innovation, which is a way of managing innovation in stark contrast to the traditional management of company research laboratories, distinguished by the secrecy of discoveries and simulation, methodologies that use machine learning are adopted to support the decision-making model and to assist researchers in calculations and simulation. It comprises a mindset, a method of thinking

about research and development in the age of information and globalisation that is built on openness, where a licence to be downloaded and utilised is strictly required.

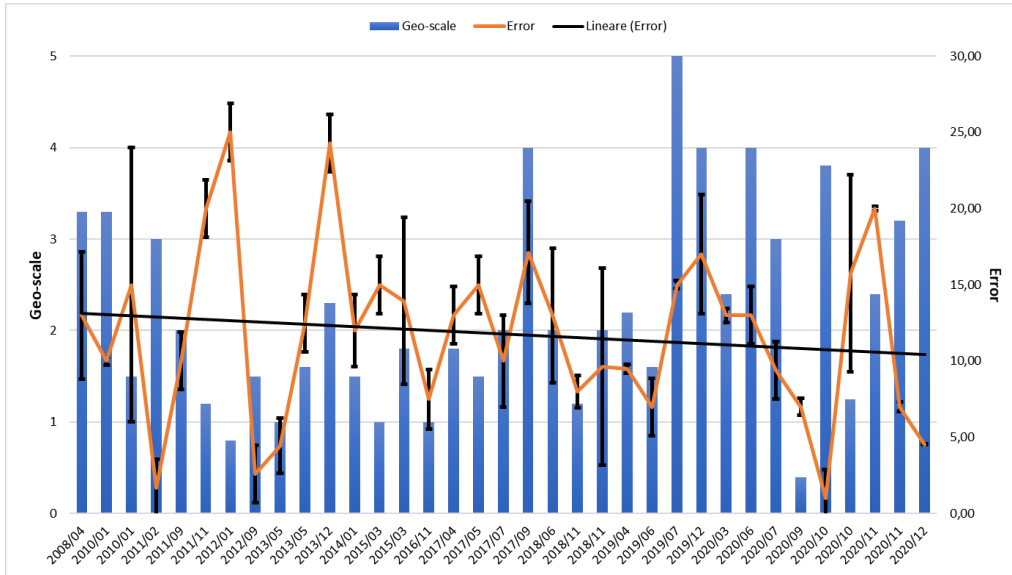


Figure 14 Decreasing trendline of error with respect to the years that studies were accomplished

## **2.4 Solar Photovoltaics**

Solar photovoltaics are described in various ways in different articles. One of the many says that it is the direct conversion of sunlight into electricity. It can be specified as the energy based on semiconductor technology that converts sunlight into electricity. The overall review highlights that it is the direct conversation of radiation into electricity.

### **2.4.1 Solar PV Applications**

Solar PVs offer a wide range of uses. This section summarises these applications. For starters, they are employed in the spacecraft industry. Photovoltaic energy is turned into electrical energy for use in spaceship on-board systems. Gallium arsenide cells, although being more expensive than silicon cells, are the primary technology employed in this application. [74]

Solar PVs are also employed in water pumping applications. Well and river water pumping is utilised in farms for irrigation of crops, livestock, and residential consumption. They are used to illuminate parking spots, signs, and other outdoor locations in roadways.[75]

Photovoltaic panels are often positioned in the lighting structure or built into the pole itself, and they contain a rechargeable battery that powers the bulbs. There is no need to create ditches, install wiring, or make other preparations for typical lighting systems. [76]

It is used at isolated telecommunication stations to generate power for the operation of equipment like as communication radios, radio communication devices, telemetry stations, public telephones, PLCs, and video cameras. Provides dependability and minimum maintenance. [74]

Water desalination (the conversion of saltwater into potable water) is another use that can be considered. This is done using batteries that are charged throughout the day with solar panels.[74]

Solar panels used in satellites are made up of solar cells situated on the spacecraft's exterior surfaces, which can be affixed to the satellite body or left open and orientated to the Sun. Currently, three-junction solar cells are utilised in series (called a triple junction). With a germanium foundation. Because of their position, they can receive more photons than panels deployed on Earth and provide more energy to keep the satellite's electrical equipment working. All measurement equipment, weather sensors, processing, and communication are powered by the solar panel.[77]

Building integrated photovoltaic systems are a collection of solar systems and technologies that are incorporated into the building and form part of its exterior coverings such as roofs and facades. Are architecturally incorporated into the building design and regarded as a functional aspect of the building structure. Serving as both a building envelope material and a power producer.[74]

## 2.4.2 Photovoltaic Cell Technologies

Some conditions must be met for a solar cell material to be regarded ideal: bandgap among 1.1 and 1.7 eV, since the smaller the gap, the easier it is to promote an electron from one band to the other, increasing the conduction of this material; made of readily available, non-toxic materials; simple fabrication method, ideal for large production volumes; high photovoltaic conversion efficiency; long-term stability A material that meets all of the parameters has yet to be discovered.[78]

First generation photovoltaic systems (completely commercial) that employ crystalline silicon (c-Si) technology in both its simple crystal-line and multicrystalline forms (mc-Si). [79]

Thin-film photovoltaic technologies are used in second generation photovoltaic systems, which are divided into three main families: (1) amorphous silicon (a-Si) and micro amorphous silicon (a-Si /c- Si); (2) cadmium telluride (CdTe); and (3) copper indium selenide (CIS) and copper, indium gallium dieseline (CIGS). [79]

Third-generation photovoltaic systems include organic photovoltaic technologies that are still in a demonstration or have not yet been commercially commercialised, as well as innovative concepts under development.[79]

Considering organic semiconductors are less expensive than inorganic semiconductors such as silicon, organic photovoltaic cells have the long-term potential to achieve the aim of a PV technology that is economically feasible for large-scale power generation. Furthermore, organic molecules may be treated using simpler processes that are incompatible with crystalline inorganic semiconductors. [79,80]

# Chapter 3

## 3. Methodology

### 3.1 Preliminary data collection and preparation

Since the accuracy of the final result depends on the accuracy of the original data, the collecting of the various data is the first step of the analysis, which is of essential importance. Two key input data may be identified as the meteorological data and the territorial data in order to execute the analysis and achieve the thesis's goal. These two datasets were created in the QGIS environment to be input for the SEBE model and to do a geographical analysis of the photovoltaic resource's accessible regions.

#### 3.1.1 Meteorological data

The SEBE model uses meteorological data as its input data, and it requires observed hourly data of shortwave radiation for a period of at least a year to produce a complete description of the input forcing conditions. The Copernicus project [55] datasets offered by the "Ladybug tools" have been chosen as the source of the data with the intention of making environmental design information and tools freely available to any individual, project, and design process.[56]

The following meteorological input data are required for the SEBE model's calculations:

- Incoming/global software radiation [ $\text{W}/\text{m}^2$ ]
- Diffuse software radiation [ $\text{W}/\text{m}^2$ ]
- Direct software radiation [ $\text{W}/\text{m}^2$ ]
- Air temperature [ $^{\circ}\text{C}$ ]
- Relative humidity[%]
- Time related variable (year, days of the year, hours, minutes)

The aforementioned information is given by Italian datasets, and the UMEP pre-processing program should prepare it before it can be applied with SEBE.

### 3.1.2 Territorial data

Calculating the PV technical potential requires accurate territorial GIS data. Numerous open sources with public geoportals provide high-resolution geospatial data for Italian territory at the national, regional, and local levels. Digital Terrain Models and high resolution Digital Surface Models are two examples of the essential territory maps.

High-resolution DSMs are crucial for providing precise estimates of the solar radiation on roofs and ground surfaces. They include the key data inputs for the SEBE model simulation, such as buildings and ground heights. The distinction between a DSM and a DTM (Digital Terrain Model) must be made first, and this comparison will be made in depth in the QGIS section. [61]

The high-resolution DSMs are not present in the SITR geodatabase, but they are available on the national geoportal run by the Italian Ministry of Ecological Transition. A DSM grid resolution of 2 metres and 0.5 metres has been employed in this thesis.

It was essential to send a formal request by mail to the Ministry to receive the appropriate DSMs, and then to wait for the credential needed to download the data. The surveyed area is divided into many rasters, each of which is represented by a separate DSM.

### 3.1.3 Slope

A slope map demonstrates the steepness of slope for the surface. Reclassify tool was used to categorise the slope map and 9 different classes of slope values were assigned to complete the map. The classes utilised for the slope map are listed below. [81]

- 0 thru 10 = 1
- 10 thru 20 = 2
- 20 thru 30 = 3
- 30 thru 40 = 4
- 40 thru 50 = 5
- 50 thru 60 = 6
- 60 thru 70 = 7
- 70 thru 80 = 8
- 80 thru 90 = 9

From 0° to 90°, the 9 slope classes were equally divided into groups of 10°. Only the flat and south-facing pixels remained after the reclassification; the spots with slopes more than 60 degrees were eliminated as being unsuitable for PV installation. Additionally, they were removed, including information from roads and trees, by using the software's built-in building footprints as it was explained in the workflow.

### 3.1.4 Aspect

An aspect map shows the direction of slope for the continuing surface. The aspect map was reclassified using the reclassify tool. 7 classes assigned for aspect are listed as follows:

- 0 thru 45 = 1
- 45 thru 90 = 2
- 90 thru 135 = 3
- 135 thru 180 = 4
- 180 thru 225 = 5
- 225 thru 270 = 6
- 270 thru 315 = 7
- 315 thru 359.5 = 1

This enables the grouping of regions with similar exposure and slope. The four aspect classes were 315° - 45°, 45° - 135°, 135° - 225°, and 225° - 315°, which stood for North, East, South, and West. We tried to pay attention to the pixels with a null (zero) value, which are to be considered towards the South rather than the North as they are painful but in any case conducive to the installation of photovoltaic panels. [81]

### 3.1.5 Principle of Solar Radiation

The quantity of energy generated by the sun is referred to as solar energy or solar radiation. The amount of solar radiation collected by the Earth fluctuates from day to day owing to differences in the spectral spectrum induced by solar activity and atmospheric attenuation [89]. Direct, diffuse, and reflected solar radiation are the three forms of solar radiation spectrum that reach the Earth's surface. Figure 15 depicts an instance of direct, diffuse, and reflected solar radiation.

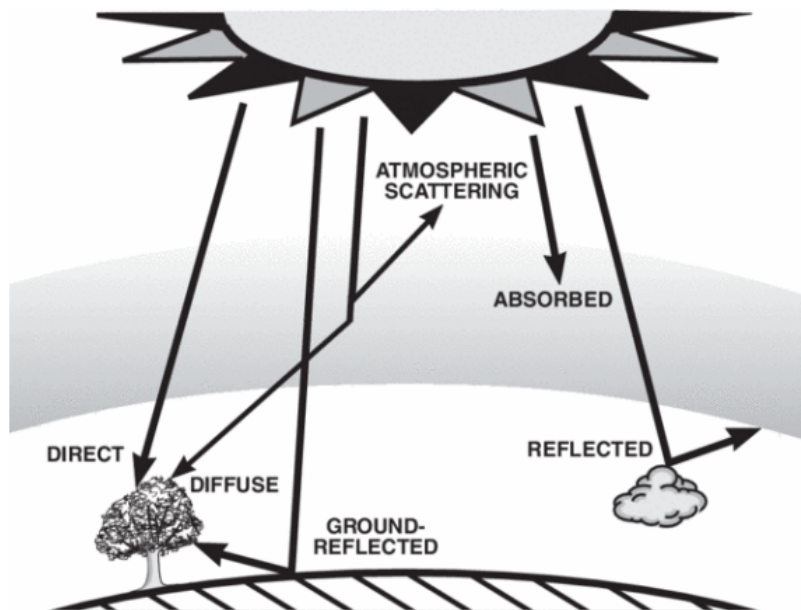


Figure 15 Direct, diffuse and reflected solar radiation [82]

The solar energy that reaches the Earth's surface without being dispersed by the atmosphere is referred to as direct solar radiation. As elevation decreases, direct solar radiation decreases, and as solar radiation goes through the atmosphere, the farther it travels to the lower surface elevation, the more effect from water vapour, aerosol, and mixed gas, and therefore the attenuation is greater [83]. This process influences solar radiation, which is referred to as diffuse solar radiation. Reflected radiation is the quantity of solar radiation reflected off the Earth's surface, which has a minor percentage and is frequently overlooked in solar radiation calculations [84]. Global solar radiation, or GHI, is the sum of the direct, diffuse, and reflected components, and it is employed in most methods to compute the overall quantity of solar radiation.

Solar energy is typically stated in the literature using two terminologies: irradiance and irradiation. The former is the instantaneous solar energy received by the Earth's surface per unit time ( $\text{W}/\text{m}^2$ ). [85] The latter phrase refers to the quantity of solar energy that falls on a specific area in a given period ( $\text{Wh}/\text{m}^2$ ). [85]

The seasons on Earth are not determined by the Earth's proximity to the Sun. Every year, the Earth is closest to the Sun on or around January the first and farthest away

on or around July the first. The seasons are caused by the amount of solar energy that reaches the Earth.

The quantity of energy emitted by the Sun remains constant. Insolation is the term used to describe the incoming sun radiation. Seventy percent of solar energy reaches the Earth. The Earth's surface absorbs 51% of the insolation. Water vapour and dust absorb 16 percent of the total energy.

The remaining 3% is absorbed by clouds. 6 percent of the 30 percent reflected back into space is reflected by air and dust. Clouds reflect 20% of the light, while the surface reflects the remaining 4%. The absorbed energy can be reradiated. Seventy percent of the reradiated energy is lost to space. The surface accounts for 21% of this, with the atmosphere accounting for the remaining 49%. The remaining 30% is transported to the atmosphere via the surface.

### 3.1.6 Equinoxes and summer and winter Solstices

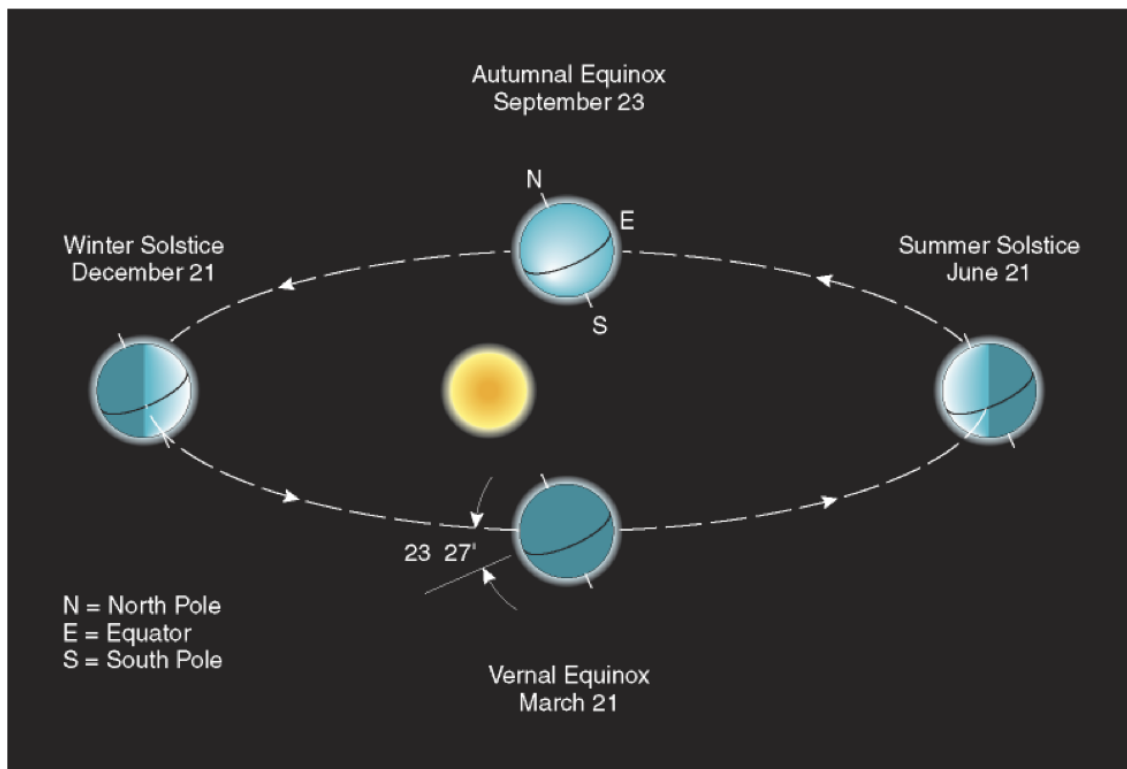


Figure 16 The orbit of the Earth relative to the Sun [90]

The amount of solar energy received at Earth's surface is determined by the length of the daylight period and the passage of the Sun across the local sky. Earth's axis is perpendicular to the Sun's beams twice a year as it travels around the centre of the solar

system. This occurs on the Spring (Vernal) Equinox, which occurs on or around March 21st, and the Autumn (Autumnal) Equinox, which occurs on or around September 23rd. Terminology is skewed toward the Northern Hemisphere.[86]

There are two instances when the Earth's axis is the greatest inclined from perpendicular to the Sun's beams. These are the solstices, which occur roughly halfway between the equinoxes.

On June 21st, the North Pole is inclined 23.5 degrees from the vertical and tilted toward the Sun. The subsolar point is located at 23.5 °N. At this period, more than half of the Northern Hemisphere is lighted at any given moment, resulting in daytime durations of more than 12 hours.[86]

For the Winter Solstice, which occurs on or around December 21st, the Earth's axis is also inclined 23.5 degrees from perpendicular to the Sun's beams. The subsolar point, however, is at 23.5 °S at this time of year. The North Pole tilts away from the Sun, and no radiation reaches the Arctic Circle (66.5 degrees North). Less than half of the Northern Hemisphere is lighted, and daylight hours are less than 12 hours.[86]

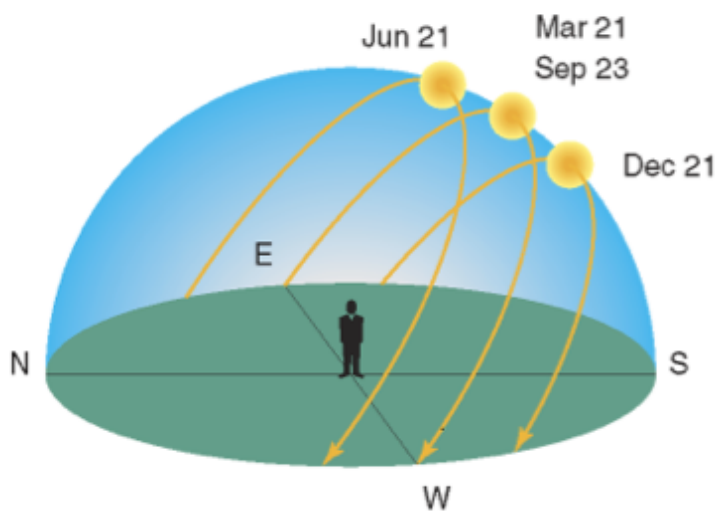


*Figure 17 Sun path at Northern Hemisphere [90]*

The figure above demonstrates the Sky Views of the Sun depicts the impact of rotation, revolution, and axis orientation on the passage of the Sun through the sky at various times of the year. [86]

The Sun's passage across the local sky and the length of daylight work together to create variable quantities of solar energy reaching Earth's surface. The amount of energy received is a crucial component in shaping the character of meteorological conditions and, ultimately, the climate of an area. In general, the higher the latitude, the wider the

range that is the difference between maximum and minimum in solar energy received throughout the year and the greater the seasonal variation.[86]

Solar radiation is not received in the same way everywhere on Earth's surface, owing mostly to astronomical causes. Astronomical considerations do not provide a complete picture of sunshine and seasons. The daily variations in solar energy received at Earth's surface during each season are caused mostly by the interaction of the radiation with the atmosphere through which it passes.[86]

## **3.2 Tools and Software**

The European Conference of Ministers Responsible for Regional Planning (CEMAT) approved the following definition of spatial planning: "Regional/spatial planning is at the same time a scientific discipline, an administrative technique, and a policy developed as an interdisciplinary and comprehensive approach directed towards a balanced regional development and provides geographical expression to the economic, social, cultural, and ecological policies of society [57]

The term "spatial planning systems" actually refers to a strategy used by the public and private sectors to manage the distribution of people and activities over a variety of scales. The aim is to achieve social and economic objectives while achieving a more logical territorial arrangement of land use and the connections between them[58]. By balancing the need for growth with the need to protect the environment, this will be accomplished. Therefore, it is essential to encourage sustainable expansion while improving quality of life through spatial planning.

The environmental and landscape implications may be considered early on in a project when the spatial planning approach is used by the energy industry, for example, when selecting the best areas to build renewable energy plants. This increases the possibility that projects will be approved or, in this case, enables a more accurate estimation of the energy potential in a certain location.

## 3.2.1 QGIS

### 3.2.1.1 Description and functionality

A free and open-source geographic information system is called QGIS (GIS). The GIS tool is employed by showing, producing, and analysing geographical data in order to resolve real-world issues. GIS's core library includes all of its features, and an analysis library built on top of it makes it possible to carry out geographic analyses on both raster and vector data. Through its simple-to-use graphical user interface, QGIS attempts to be user-friendly (GUI). QGIS synthesises maps with data tables associated properties. components of the server library retrieved through mapping. A project may be thought of as a collection of 2D and 3D vector and raster data. The following are some vector data formats: GeoPackage, ESRI shapefile, SDTS, and GML.[59]

### 3.2.1.2 WMS and WFS

Online geographic data is acquired with OGC Web Services including Web Feature Services and Web Map Services (WFS). Image files are often downloaded from WMS servers in the TIFF format. Contrarily, vector files are made available via WFS servers and may be used to import points, polygons, and polylines to generate base map layers. As a result, they offer properties and features like geometry for use in geospatial analysis [59]. In order to better visualise and alter the projection of our raster maps and to verify that everything is aligned properly, we utilised this service to upload Google Satellite to the maps.

### 3.2.1.3 DTM, DSM, and DEM



*Figure 18 Continuous black line represents the DTM whilst the DSM is showed as dashed red line [60]*

The spatial datasets known as digital elevation models (DEM) are digital collections of ground elevation used to display topography. Digital elevation model (DEM), digital surface model (DSM), and digital terrain model are the three primary categories into which they may be divided (DTM). A DEM is a surface model devoid of any non-ground features, such as trees and buildings. DTM is a subset of DTMs and is a generic model that consists of one or more forms of terrain information. DSM is an elevation model that includes the ground and everything on it.[61]

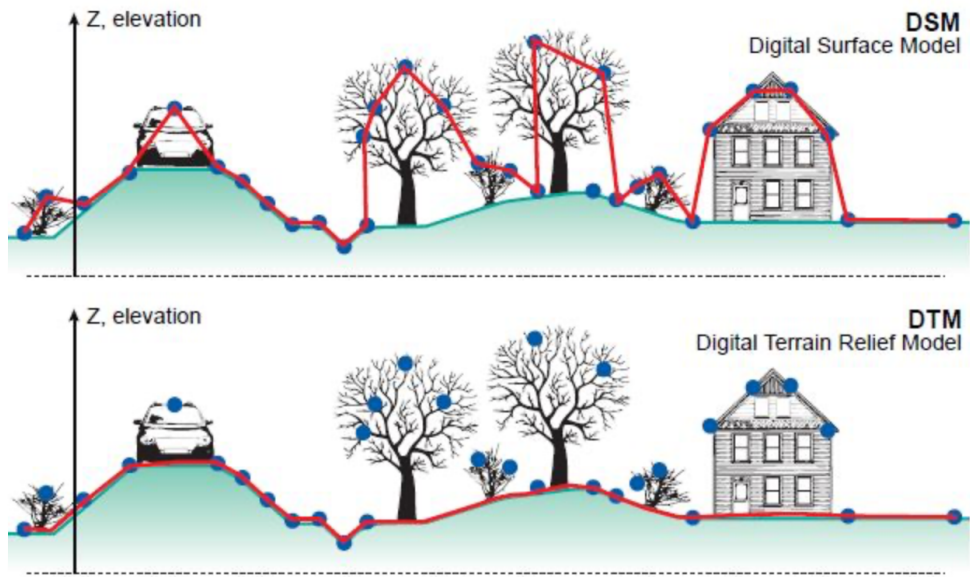


Figure 19 DSM and DTM comparison [60]

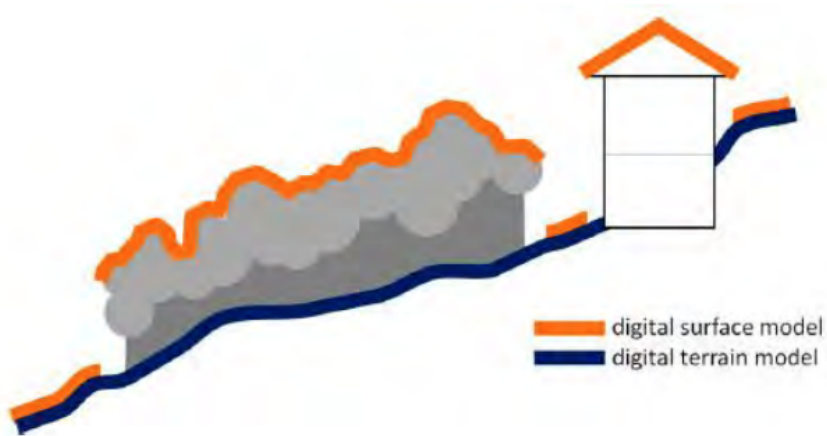
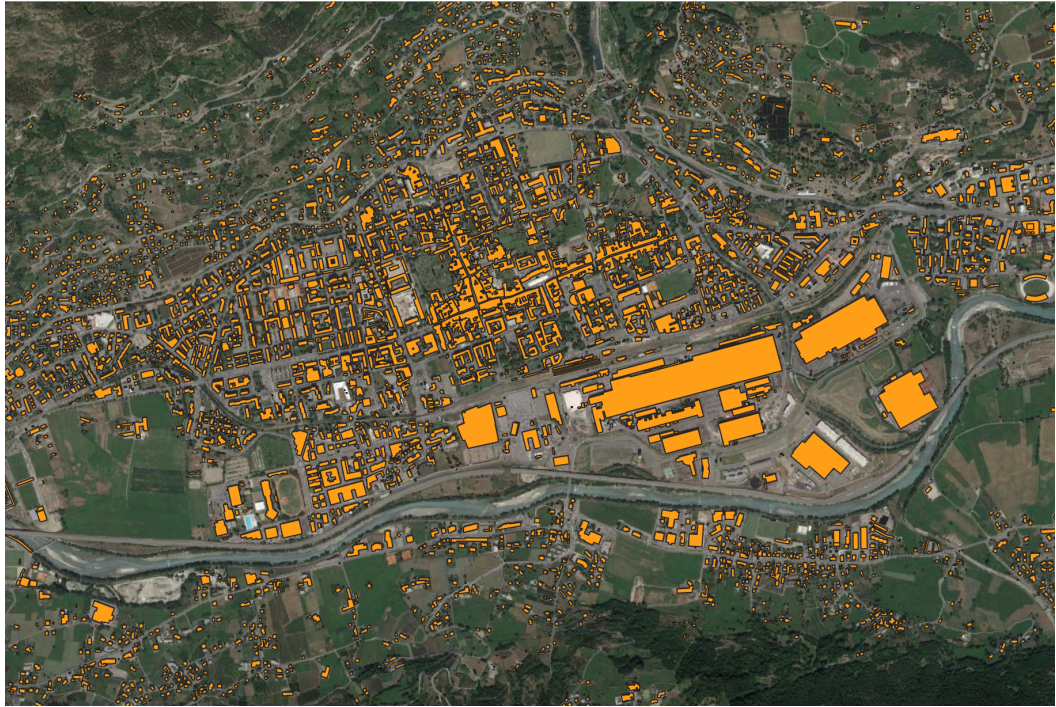


Figure 20 Digital Surface Model vs Digital Terrain Model [87]



*Figure 21 Building footprints of Aosta*

To create the wall heights and wall aspects needed to calculate the irradiance on building walls by using the "Wall Height and Aspect" function in the urban geometry tool of the UMEP pre-processor plugin. These data are already included in the DSM raster files.

#### **3.1.2.4 Graphical modeller**

The bulk of analytical activities are incorporated into processes rather than being completed separately in QGIS. The procedures to develop a model and how to utilise it will be covered in the following subchapters. The graphical modeller may be used to combine that group of processes into a single process, making it simple and beneficial to run that process later on with a new set of inputs.[59]

### 3.1.2.5. QGIS CRS

#### 3.1.2.5.1. Working with Projections

For layers that do not have a specified CRS, QGIS allows users to establish a global and project-wide CRS (coordinate reference system). It also allows the user to establish custom coordinate reference systems and supports vector and raster layer on-the-fly (OTF) projection. All of these characteristics enable the user to display layers with varying CRSs and have them overlay correctly.

#### 3.1.2.5.2. Overview of Projection Support

QGIS now supports around 2,700 recognised CRSs. The definitions for each CRS are saved in a SQLite database that comes with QGIS. Normally, you do not need to directly edit the database. In fact, doing so may result in the failure of projection assistance. A user database stores custom CRSs. For details on maintaining your own coordinate reference systems, see the section Custom Coordinate Reference System.

The CRSs offered in QGIS are based on those specified by the European Petroleum Search Group (EPSG) and the Institut Geographique National de France (IGNF), and are mostly abstracted from GDAL's spatial reference tables. The database contains EPSG IDs, which may be used to declare a CRS in QGIS.

To utilise OTF projection, your data must either contain information about the coordinate reference system or you must establish a global, layer, or project-wide CRS. QGIS utilises the spatial reference identifier supplied when the layer was generated for PostGIS layers. QGIS relies on the availability of a recognised mechanism of expressing the CRS for data provided by OGR. In the context of shapefiles, this indicates a file that contains the CRS's well-known text (WKT) specification.

Recently Used Coordinate Reference Systems	
Coordinate Reference System	Authority ID
ED50 UTM fuseau 32	IGNF:ED50UTM32

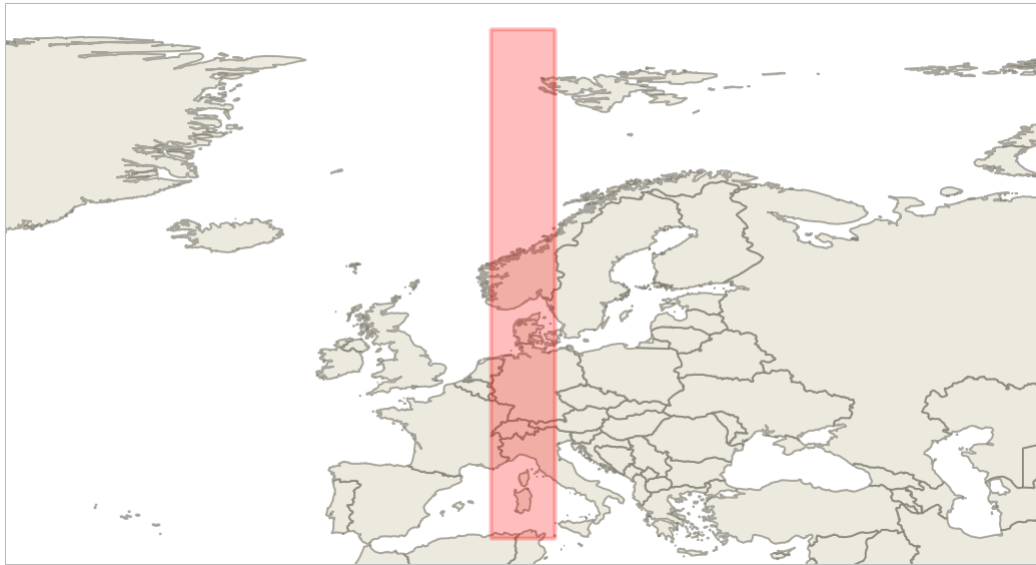


*Figure 22 CRS for Aosta Simulations*

ED50UTM fuseau 32 was used for Aosta simulations as CRS as represented in the figure above. ED50 demonstrates the Geodetic CRS as well as the prime meridian is Greenwich and the ellipsoid is International 1924. Information source of the CRS is IGNF that is a French company provides a shift grid for transforming the geodetic systems NTF to RGF93 [88]

### **3.2.2 UMEP**

A tool for urban climate services called UMEP (Urban Multi-scale Environmental Predictor) combines models with sensitive planning primarily for climate simulations. In addition to being primarily used for applications related to outdoor thermal comfort, urban energy consumption, and climate change mitigation, there are many interesting applications, such as the impact of green infrastructure on the urban context, the effects of buildings on people's thermal stress, and the impact of human activities on heat emissions. These applications allow for simulations, scenario planning, and the comparison and visualisation of various combinations of climate indicators. UMEP is designed to be quickly updated when new features are generated and to be openly accessible to researchers, decision-makers, and practitioners as an open-source tool that is entirely available on github (including the developer version).[59]

To avoid having to buy any rights or licences, the community developed the open source UMEP plugin for QGIS, which is used to enhance modelling capabilities. The

major purpose is to give users the ability to link geographical data with the goal of defining model parameters.[59]

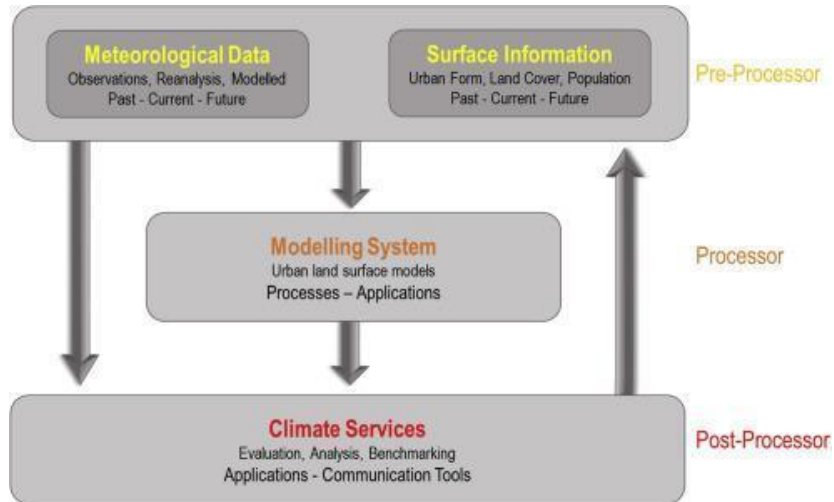
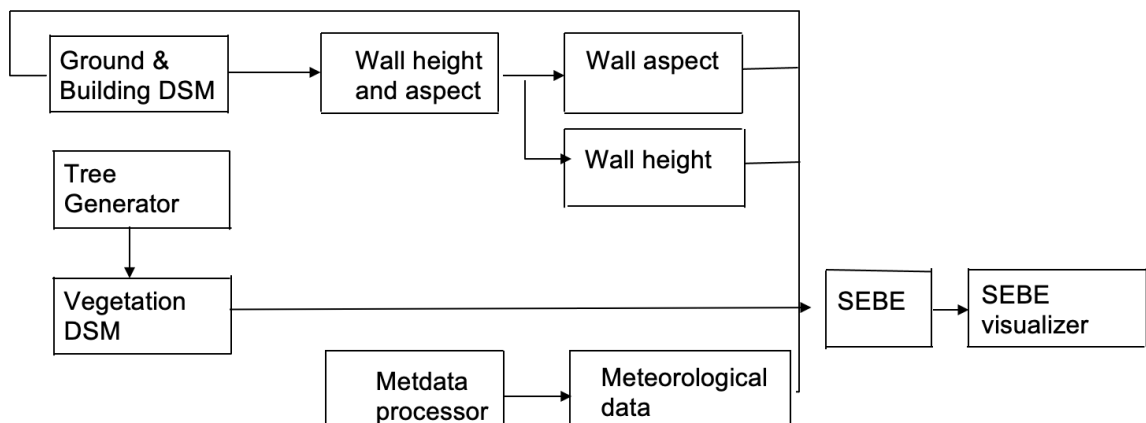


Figure 23 Processors of UMEP plugin classification[59]

The UMEP plugin components that interest us are pre-processing, processing, and post-processing. The purpose of pre-processing is to get the geographical and meteorological data ready for the system's inputs. All the major models for computations are covered by processor features. A post-processor feature is utilised to plot the findings and offer rapid glances.[59]



*Figure 24 Workflow of solar irradiance analysis on building envelopes using SEBE model with necessary geodata[59]*

### **3.2.2.1 Solar Energy on Building Envelopes (SEBE)**

The most helpful UMEP plugin function, known as SEBE, is used to visualise prospective solar energy generation (Solar Energy on Building Envelopes). It has the ability to compute irradiances at the pixel level, allowing it to estimate potential solar energy on building walls and roofs using a 2.5-dimensional model of the ground and a digital surface model of the building (DSM). [59]

The total irradiance for a roof pixel "R" may be calculated by adding the radiation that is direct ("IωS"), diffuse ("DS"), and reflected ("G(1-S)α").[59]

$$R = \sum_{i=0}^p [(I\omega S + DS + G(1 - S)\alpha)]$$

The shadow "S" calculated for each pixel is evaluated as:

$$S = Sb - (1 - Sv)(1 - \tau)$$

Shortwave radiation transmissivity is expressed by "τ" whereas building shadows ("Sb") and vegetation ("Sv") are indicated by presence ("0") or absence ("1"). The shortwave radiation fluxes may be overestimated or underestimated as a result of SEBE's hourly radiation emphasis.[59]

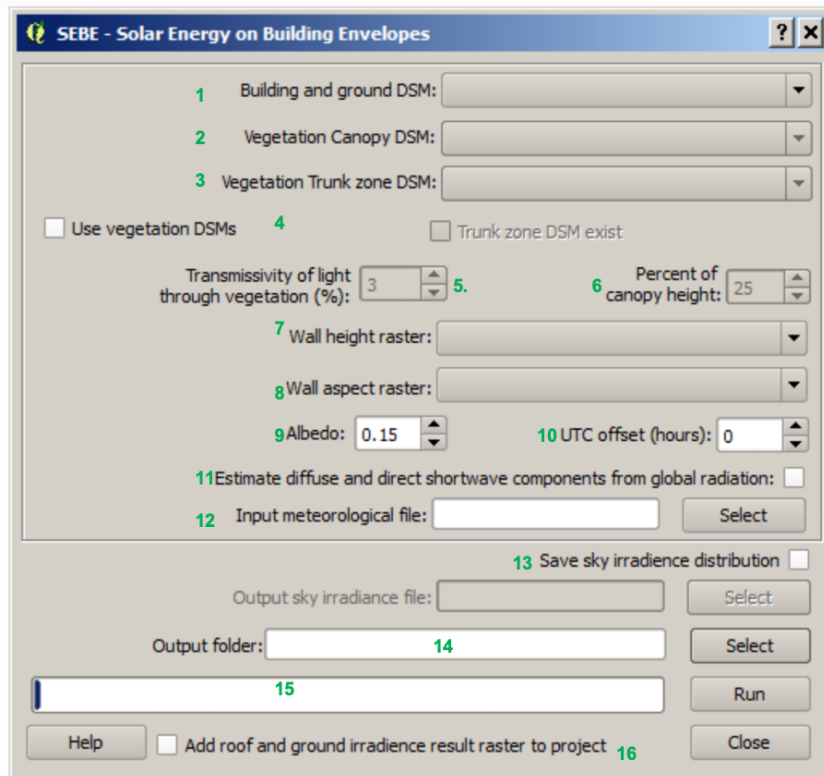


Figure 25 Solar Energy on Building Envelopes [59]

Beginning with step one and continuing until step six, the box includes the introduced input data. After the seventh step, the user must choose the output folder where they wish to store the output files and specify how to use them. [59]

- **Building and ground DSM:** To choose the DSM file containing building and ground heights, click the box labelled with number 1. The latitude and longitude used to calculate the location of the sun are also included in the chosen DSM file.[59]
- **Use vegetation DSMs:** If this box is checked, two vegetation DSMs are required. The first vegetation DSM (Vegetation Canopy DSM) describes the top of the vegetation, and the second one the bottom that lies below the canopies (Vegetation Trunk Zone DSM). Vegetation data reduces potential solar energy by casting shadows on the ground, walls, and roofs. As a result, overestimating solar irradiation might result from ignoring vegetation data.[59]
- **Wall height and Wall aspect raster:** The high-resolution DSM referenced in the first box above has created two raster files that, respectively, include the wall

heights and wall aspects of the structures. These two rasters must be obtained in order to calculate the irradiance on building walls. [59]

- **Albedo:** The albedo box determines the reflectivity of shortwave radiation of all surfaces defined in the vegetation DSM section, including the ground, roofs, walls, and plants. For all surfaces, the albedo is set to an average value of 0,15. (Lindberg, 2015) [59]
- **UTC offset (hours):** In order to correctly specify the location of the sun, UTC offset is employed. If the ERA5 dataset is included, UTC is set to 0 since it is associated with the meteorological forcing data. [59]
- **Input meteorological file:** Select and add the input meteorological file to the project here. This meteorological file must be in the correct format to be utilised with UMEP. As indicated in the introduction section of the preliminary data preparation, a dataset with an average length of one year and hourly time resolution should be employed for SEBE.[59]
- **Output folder:** This box should be checked to specify the user-specific folder where results are saved. Following this procedure, there will be two output files: one raster file displaying the irradiance on the ground and building roofs, and the other as a text file displaying the irradiance on walls.[59]
- **Add roof and ground irradiance result raster to the project:** When this box is checked, the output is immediately uploaded to the QGIS map canvas interface.[59]
- **Run:** This box begins the computationally difficult computations related to the DSM's resolution and extension.[59]

If the model operates without a problem, three necessary datasets are saved as outputs:

- The pixel-by-pixel total irradiance in kWh, including on the ground and rooftops, is displayed in the geoTIFF **Energyyearroof.tif**. [59]
- The simulated grid is represented by the first and second columns of the text file **Energyyearwall.txt**, while the remaining columns show the irradiance values for each wall voxel starting at the bottom and progressing higher as going right in each row. [59]
- If the vegetation DSMs were included, a second file called **Vegetationdata.txt** that provides information on the height and position of the vegetation is also included. The SEBE visualisation plugin is used with this vegetation file.[59]

### 3.2.2.2 Graphical modeller

In QGIS, the majority of analytical tasks are integrated into a process rather than being performed individually. Using the graphical modeller, this collection of processes may be integrated into a single process that can then be performed later with a different set of inputs, optimising the entire process while cutting down on work time. No matter how many steps a model has, it may be run as a single algorithm, which saves time and effort, especially for bigger models. Because of this, graphical modeller's simple and user-friendly interface lets users build complex models. [59]

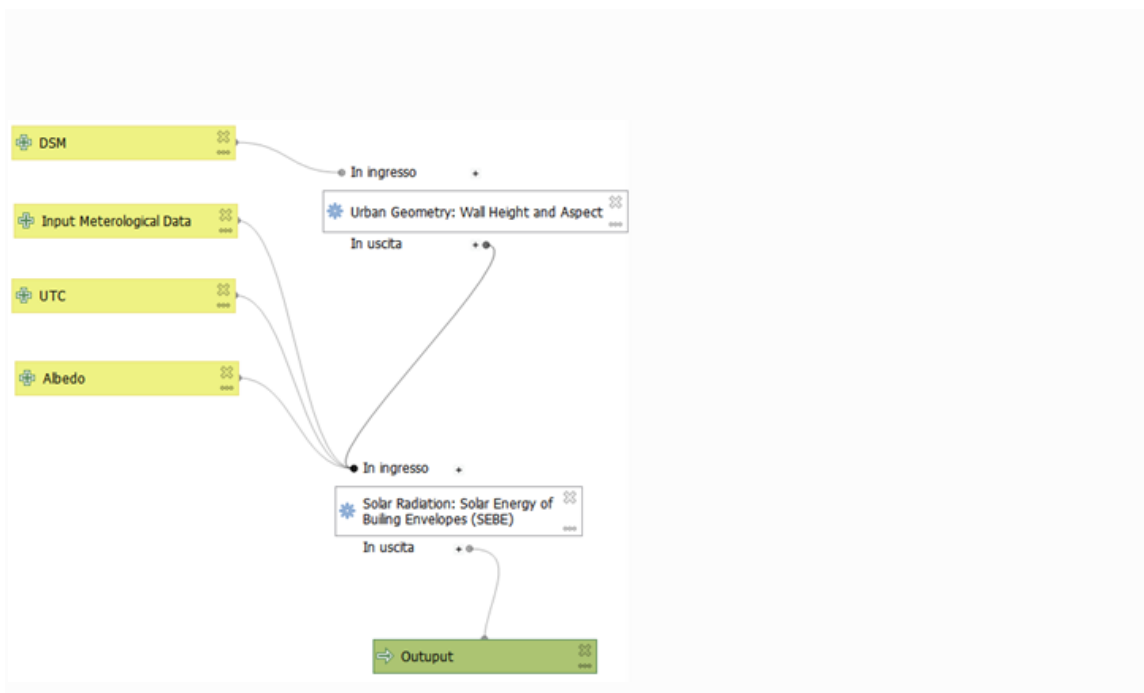


Figure 26 Graphical modeller of SEBE

The model is created in two main phases for our purposes: :

1. *Definition of necessary inputs*: These inputs will be added to the parameters window, which will be produced automatically, so that the user may adjust

their own values during the model's execution, as with all of the algorithms accessible in the processing framework. [59]

2. *Definition of the workflow*: The workflow is defined using the model input data by adding algorithms from the processing toolbox and selecting how they utilise the defined inputs or outputs provided by others in the model and how they are linked and related.[59]

A simple graphical modeller which contains the SEBE model only was presented above. In order to use the wall height and aspect function the input was selected as a DSM file. Meteorological data, UTC, and albedo were combined with the output of the wall height and aspect function and they all were used as an input for the SEBE model. Before this graphical modeller was created, all those steps should have been done separately for each map. However, for the graphical modeller, it is needed only to change the input files, and the results would be presented separately. Also it should be taken into account that this model is a simple model which consists of two functions only when we compare to the real models that takes even pages long with multiple functions.

### **3.3 Shading Analysis**

Shadow analysis was considered since it can have a major impact on the output of a solar PV system as it was clarified in the literature review section with the comparison of different methods which are currently in use. The shadow analysis used the LiDAR DSM to account for shadowing from buildings as well as any other tall objects such as trees and the landscape in general. The DSM is used as input by the Daily Shadow Pattern tool in the UMEP plugin for QGIS to build a binary raster picture representing the shadow pattern at any given moment, with 0 signifying darkened regions and 1 denoting areas that are not shadowed.[65]

#### **3.3.1 Solar Radiation, Daily Shadow Pattern**

Digital surface models (DSM) of ground and building are utilised to create pixel by pixel shadow analysis by the shadow generator plugin. Additionally, DSMs for vegetation might be employed. The source of the approach is discovered by Ratti and Richens, which is further refined and detailed in Lindberg and Grimmond (2011).[62]

PySolar, a Python module for different solar applications, calculates the Sun's position.[63],[65]

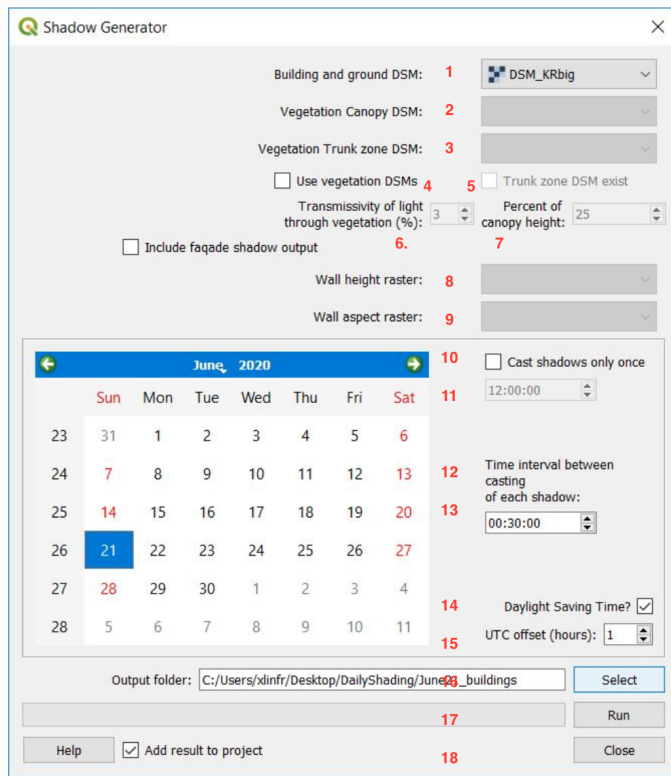


Figure 27 Solar radiation, Daily shadow pattern Dialog box[65]

- **Building and Ground DSM:** A DSM that includes both building and ground heights is called building and ground DSM. The latitude and longitude needed to calculate the location of the Sun are also determined by building and ground DSM.[65]
- **Vegetation Canopy DSM:** Different from building and ground DSM, A DSM made up of pixels with plant heights above ground is known as a "vegetation canopy DSM". It should be set to zero when there is no vegetation present. [65]
- **Vegetation Trunk Zone DSM:** A DSM made up of pixels with heights above ground for the vegetation trunk zone is named as "vegetation trunk zone DSM". The pixels should be set to zero when there is no vegetation present.[65]
- **Use vegetation DSMs:** If the user wishes to incorporate vegetation, which is trees and shrubs, when shadows are created, it should be checked using the "Use vegetation DSMs" checkbox. [65]

- **Trunk Zone DSM Exist:** If a trunk zone DSM already exists, “DSM Trunk Zone Exist” box should be ticked. [65]
- **Transmissivity of Light Through Vegetation (%):** Light Transmission Through Vegetation (%) represents the proportion of light that passes through vegetation. Konarska et al. state that 3% is the default value[64]
- **Percent of Canopy Height:** The height of the canopy DSM can be used to construct a trunk zone vegetation DSM in the absence of trunk zone vegetation DSM. The 25% setting is the default, and can be checked by percent of canopy height checkbox. [65]
- **Cast Shadows only Once:** If the user wishes to observe one specific shadow, they should tick this option. The amount of time needed to determine the sun’s position can be chosen below this checkbox. [65]
- **Specify Data:** The data should be set in the middle portion by the “specify data” checkbox.[65]
- **Time Interval between Casting of each Interval:** If the above checkbox (Cast shadows only once) is not selected, the interval-based number of shadows can be created by ticking “time interval between casting of each interval”.[65]
- **UTC offset (hours):** The time zone must be mentioned by “UTC offset (hours)”. Positive numbers are used for locations heading eastward. [65]
- **Output Folder:** The designated location where the output will be stored can be arranged by “output folder” checkbox. [65]
- **Add Results to Project:** If the “add results to project” box is ticked, the shadow raster will be included in the map canvas.[65]
- **Output:** As an output one geoTIFF will be created with pixel values of zero denoting shadow and one denoting sunlight. One shadow picture and one shadow fraction image are created if daily shadow casting is employed. Which shows that “cast shadows only once” ticked off. The shadow fraction picture is expressed as a percentage, with 100% signifying that every calculation's input pixel receives sunlight all day.[65]

### 3.4 Combination of SEBE and Shading Analysis

Shadow rasters for four different days in the year have been represented in the figure. March and June shadows are demonstrated in the top row whilst September and December are figured in the bottom row. White areas are the useful areas that are under the effect of sunlight while the black areas are under shadow during the selected days.



*Figure 28 Shadow rasters for four selected days*

4 days shadow analysis is generated by constructing a shadow pattern for each hour between dawn and sunset, and the solstices and equinoxes were selected as the 4 days to guarantee the whole range of the Sun's positions over a year was taken into account. The particular dates in consideration were March 20, June 21, September 23, and December 22, 2021. The hourly shadow rasters from each day were merged to form a continuous binary raster.

Because summer days are more important for energy generation than winter days, the allowable degree of shadowing is determined by analysing the permitted shading differently for each day of the season [66] For the months of March and September, a shadow level of 50% was determined to be adequate. For the day in June, a shading level of 40% was permitted, while a shading level of 60% was acceptable for the day in December. As a result, pixels having values less than 0.5 in March and September, 0.4 in

June, and 0.6 in December may be ineligible for the daily shadow rasters. These criteria were used to create daily binary shadow rasters by redesignating unsuitable pixels to a value of 0 and acceptable pixels to a value of 1. [67]

Yearly shadow raster was generated by multiplying the four binary rasters. As it was assigned for each binary raster, the dark pixels represent the shaded areas and equals 0 whilst the light rasters are numerically assigned to 1 and show the lit areas the whole year.

Yearly shadow raster that is the combination of for specific days was masked by using “r.mask” raster operation. Specifically “r.mask.vect” operation was used and the raster file was masked with respect to building footprint. [68]

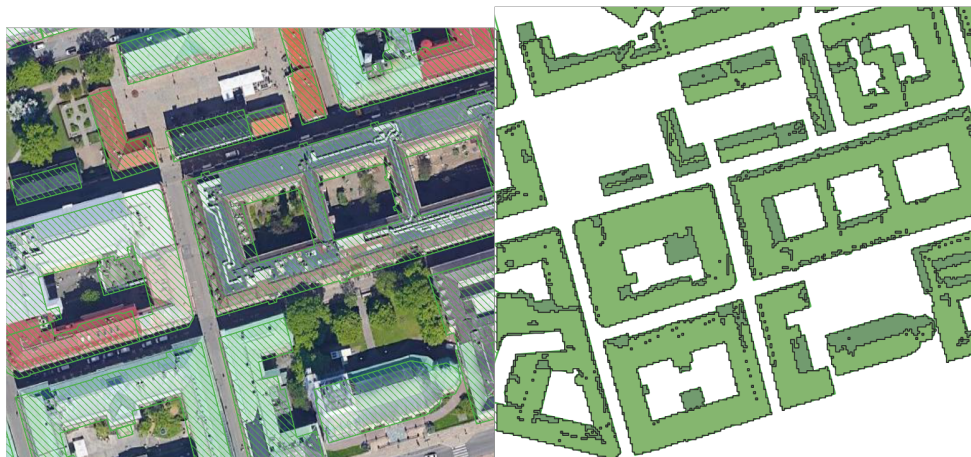


*Figure 29 Building footprints and masked vector*

Polygonization of the masked yearly shadow raster was performed by the “gdal\_polygonize.py” function. This function generates vector polygons for areas of raster pixels sharing a common pixel value. Building footprint and masked polygonized yearly shadow vector are represented in the figure. Dark polygons in the vector figure represent the shadowed areas on the rooftops and they should be eliminated to obtain the suitable areas for PV installation



*Figure 30 Suitable area polygon and SEBE application on the area*

The dark polygons were cancelled from the vector file and light polygons remained in the vector format. That new vector was used to mask the original DSM in order to use the SEBE operation. Masked final vector is placed on the left side of the figure. On the right side of the figure, the output of the SEBE operation takes place which demonstrates the technical potential of the suitable rooftop areas after shadowing analysis.

### 3.4.1 Graphical Modeller

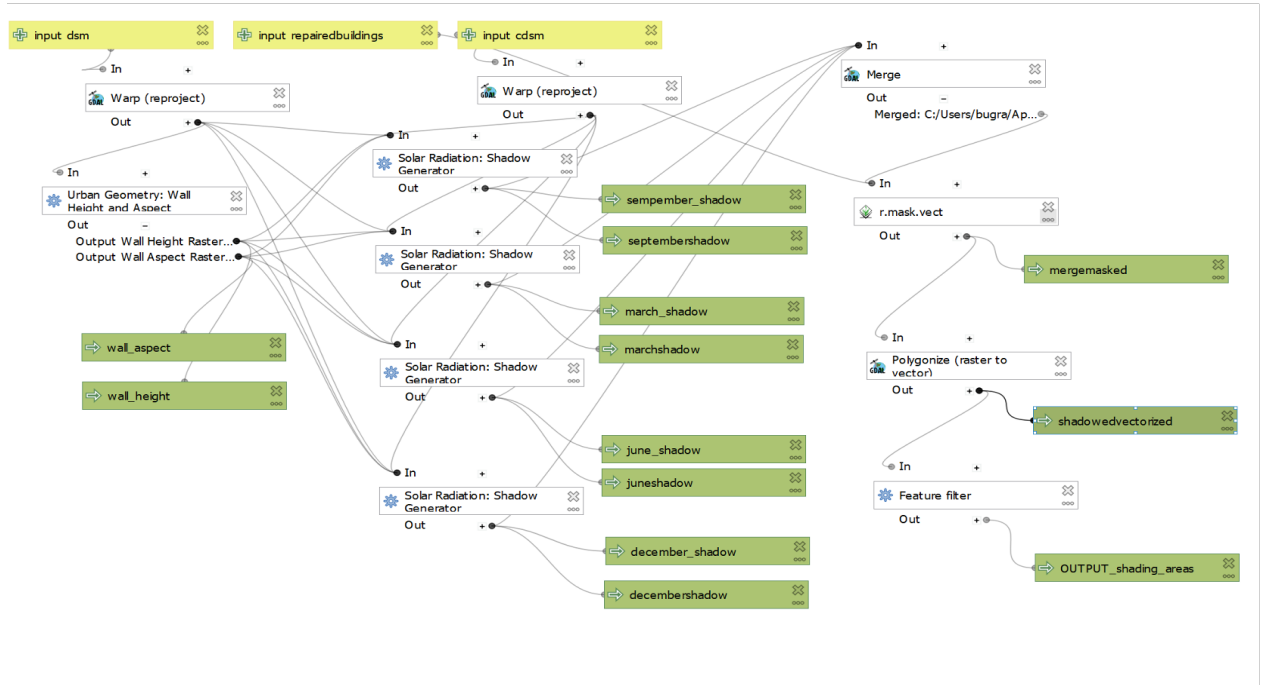


Figure 31 Graphical model of shadow analysis

Graphical model for shadowing analysis was created by graphical modeller. DSM, building footprint and canopy DSM were used as inputs for the model. Later on all the steps mentioned in this section have been performed in the order. Firstly, the wall aspect and wall height rasters were obtained by “Urban Geometry: Wall Height and Aspect” operation. Then, the outputs of urban geometry: wall height and aspect operation and canopy DSM (CDSM) were utilised as an input for “Solar Radiation: Shadow Generator” operation that is also known as Shading analysis. Later on the outputs of shading analysis were merged and one yearly shading raster was generated as an output. The model is completed with the masking operations, and the mask vector was achieved for the SEBE operation.

Graphical modeller was used in order to avoid repeating the same steps manually and to automatise the whole process for the use of future work.

# Chapter 4

## 4. Results and Discussion

### 4.1 Photovoltaic potential assessment workflow

The photovoltaic energy potential is realised using novel and scalable technology considering the shadowing effect. The assessment necessitates an assessment of usable solar radiation (physical potential), acceptable surface (geographical potential), and PV system efficiency (technical potential). The Urban Multi-scale Environmental Predictor (UMEP) plug-in is used in conjunction with a GIS-based strategy order to complete SEBE and Shadow analysis models.

The approach is separated into three basic steps:

1. Collecting geographical input data from Aosta's public geoportal (<https://geoportale.regione.vda.it/>) and data pre-processing with the QGIS toolkit and UMEP plugin.
2. Estimating solar irradiation on roofs and ground surfaces, using high and low resolution digital surface models (DSMs) and some spatial analytic manipulation to proceed with the simulation appropriately, while querying rooftop accessible segments with the solar irradiance map.
3. Estimating solar irradiance and assessing technical PV potential in appropriate places while taking system technical requirements into account.

The following graphic depicts the summary process technique for the solar energy assessment:

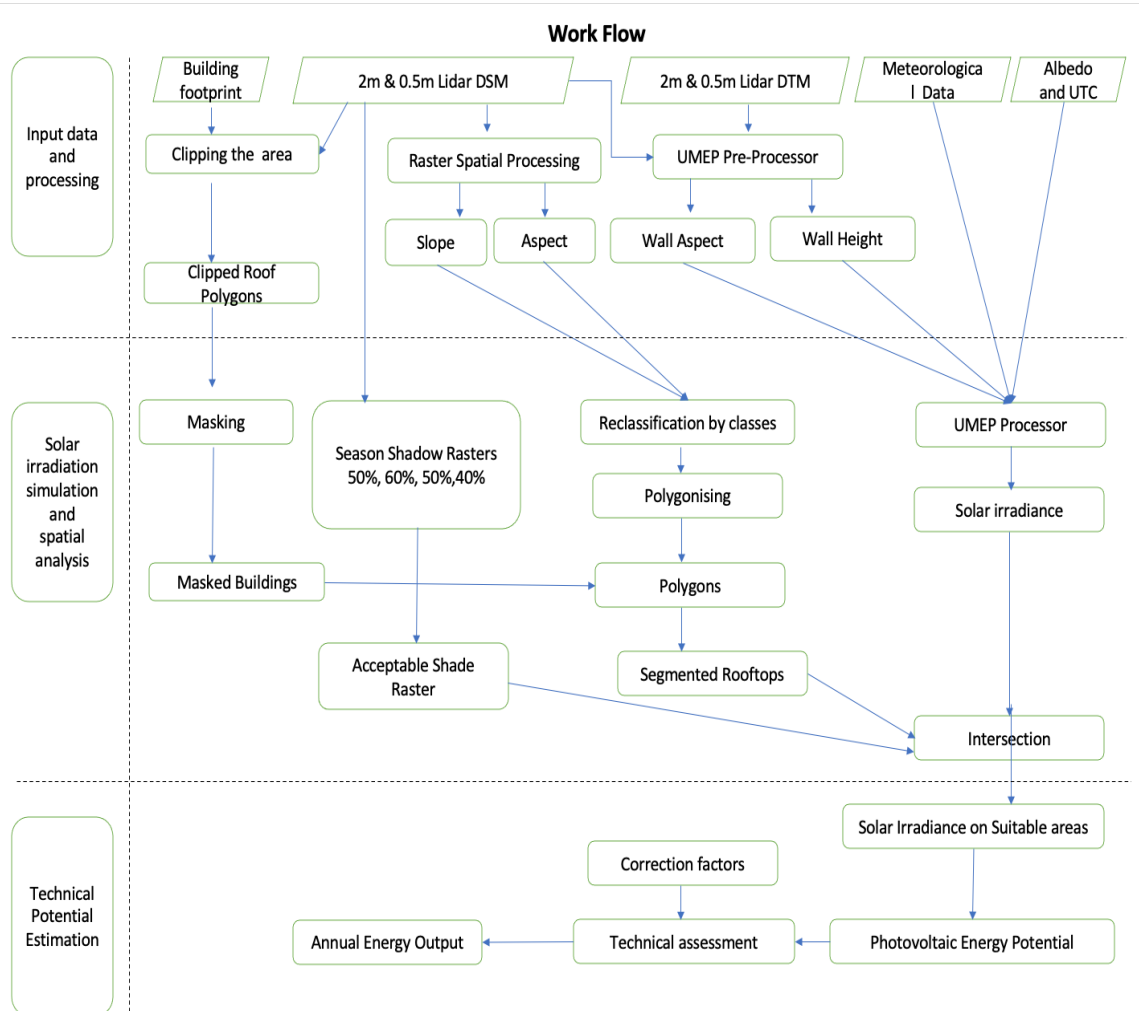


Figure 32 PV technical potential estimation workflow

The goal is to genuinely follow this procedure while attempting to describe each step as best as possible using intermediate representations. To begin, we shall run the simulator on the Aosta data with a resolution of 2.0 x 2.0 metres, followed by a focus on a narrow zone to avoid increasing the computing cost of the simulation too much, as executing it for the entire 0.5 x 0.5 metres resolution is time intensive.

### 4.1.1 Evaluation of the technical potential

The yearly potential of solar power generation at a given site may be estimated using the computed annualised solar radiation per unit surface, total usable area, and PV technology efficiency. The following equation is used to determine the yearly technical potential for photovoltaic energy:

$$E_{AC} = H_g \cdot A_{PV} \cdot \eta_{STC} \cdot PR$$

- “ $H_g$ ” represents the global solar irradiation [kWh/m<sup>2</sup>/year].
- The total area for PV electricity generation is represented as “ $A_{PV}$ ”.
- “ $\eta_{STC}$ ” is the rated efficiency of PV modules at Standard Test Condition (STC).
- The Performance Ratio is abbreviated as "PR." It compares the energy generated to the energy produced under the same amount of irradiation but under perfect no-loss conditions. It is the ratio of the final system yield to the reference yield, and it is calculated using a variety of coefficients.

### 4.1.2. Shading Analysis of Aosta

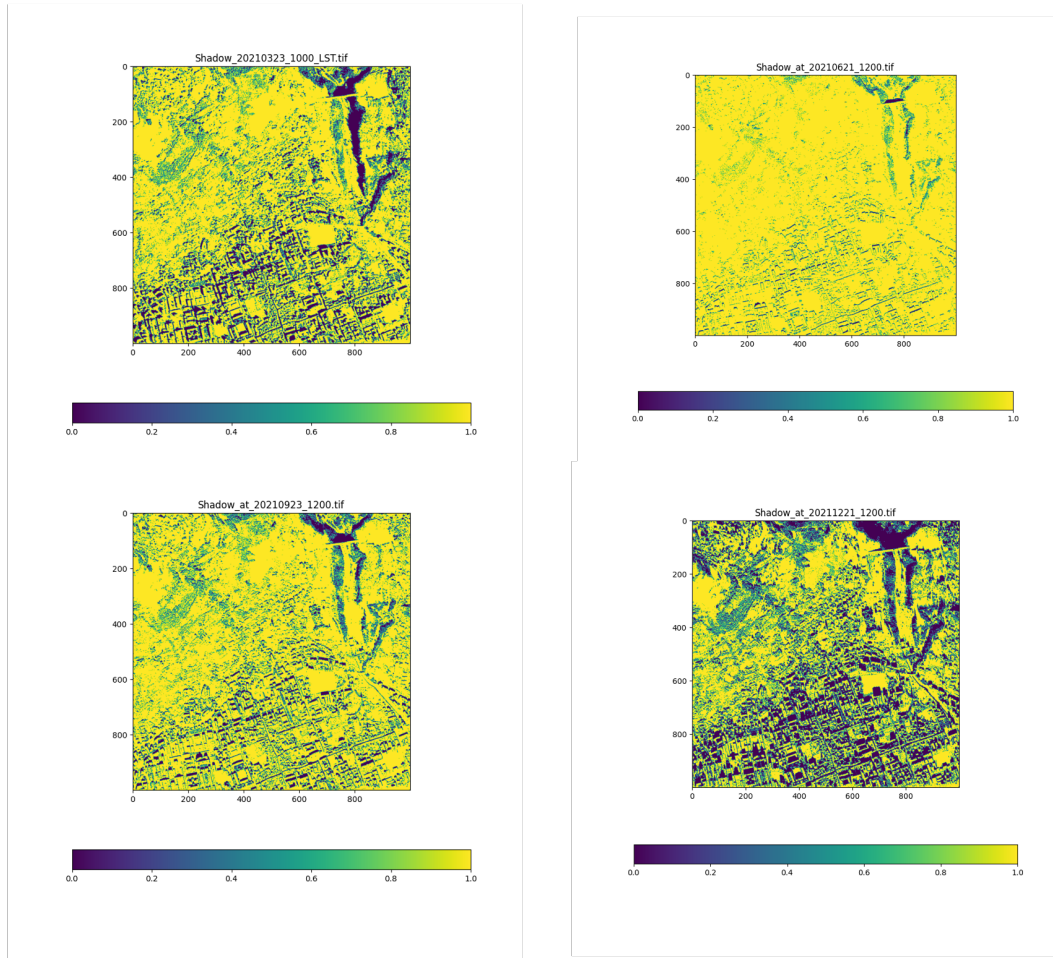
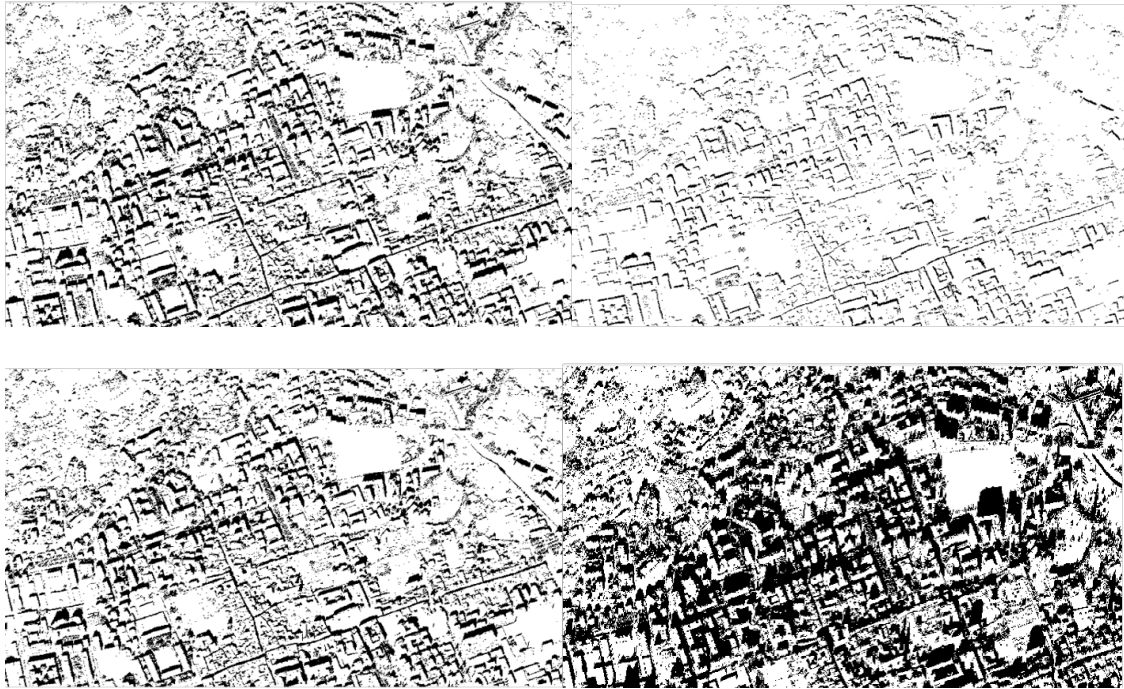


Figure 33 Shadow pattern for 4 days

The simulation of casting shadows for four specific days. Yellow represents the lit areas whilst dark purple areas are shaded during the whole day.



*Figure 34 Binary shadow rasters for 4 days in Aosta (2m)*

The binary rasters for four different days in the year have been displayed in the figure. March and June shadows are demonstrated in the top row whilst those for September and December are figured in the bottom row. While white areas are the appropriate areas for PV installation that take the value of 1, the black areas, which are under shadow during the selected days, take a value of 0 that are not appropriate.

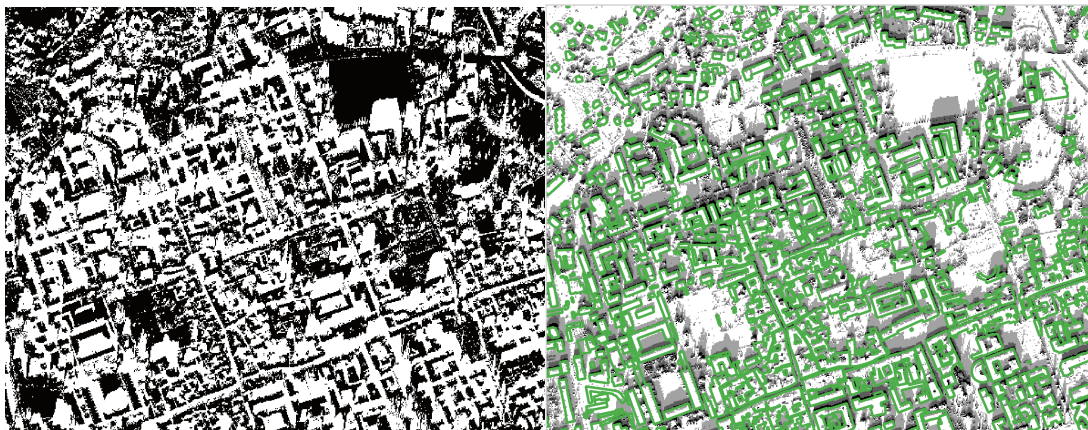


*Figure 35 Combined shadow rasters for 4 days in Aosta and building footprints on the right (2m)*

The four binary rasters were multiplied together to form the yearly shadow raster. This implies that for a pixel to be assigned a value of 1, it must have been assigned a value of 1 in all four unique rasters and is therefore appropriate throughout the whole year. Multiplication of the four shadow rasters was done by using the “r.cross” function in order to create an output raster map that consists of all unique combinations of those input rasters. Cross product results are represented in the figures above. The left figure demonstrates the output of the cross product whilst the right one is the final result after sieving the shadowed areas combined with buildings footprint.

## 4.2 SEBE and Shadow Analysis for Aosta DSM 2.0

Analysis of solar potential of Aosta were performed for two different raster resolutions that are 0.5 metres and 2 metres. The building footprint of the observed area is shown in the figure on Google Satellite map layer. In this subchapter of the thesis consists of the SEBE and shadow analysis with 2 metres resolution rasters.

ED50UTM fuseau 32 was selected as CRS of the analysis, and it was repeated for all the layer added to the project.



*Figure 36 Aosta Building footprint 2 metres DSM*

The figure below demonstrates the error for the computational time that needed to be overcome during the SEBE analysis. The same notice was present also during the shadow analysis. It was ignored for the first trials but the PC which was handling the simulations was not enough to complete the analysis should have been done. Therefore, the area of the technical solar power estimation must have been tiled and the simulations should have been performed for a reduced size area.

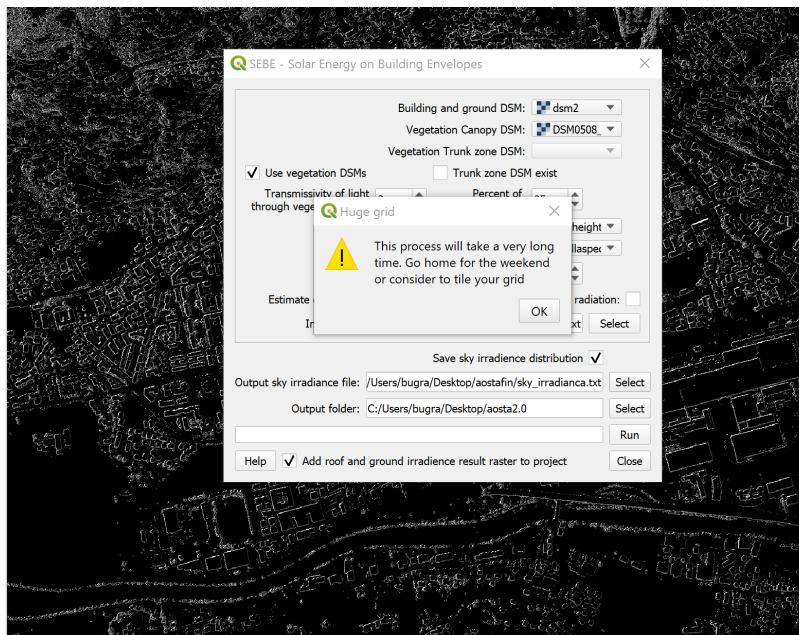
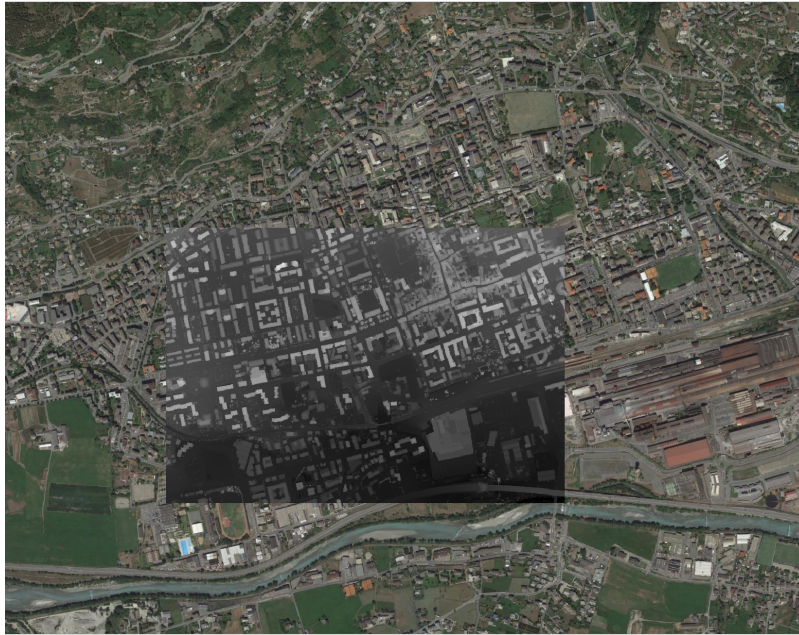


Figure 37 Aosta simulations SEBE error

The tiled DSM raster is represented in the figure below. This area was observed for the 2 metres resolutions dataset. The methodology is scalable, so the analysis could be performed in bigger areas by following the same procedure without any problems with more powerful machines.



*Figure 38 Tiled Aosta DSM*

SEBE analysis which is the analysis of solar irradiation will be performed at the end of this subchapter. Parallel to this procedure is the Raster Spatial Processing: the DSM was utilised to build an aspect raster and a slope raster, which assigns an angle to each pixel using the in-built QGIS capabilities.

The aspect and slope rasters were initially reclassified using the "r.reclass" function to reduce the whole range of aspect and slope values to 4 and 9 classes, respectively, in order to identify the roof planes. Classes are sets of values where pixels in rasters have values that are comparable. The classes for slope and aspect rasters are represented in the figure below.

The classes of the slope and aspect rasters were also mentioned in the slope and aspect subchapters in the methodology section. Slope and aspect layers were created using DSM raster of the Aosta dataset and they were reclassified in order to group the datasets and to eliminate the unnecessary data easily.

This enables the grouping of regions with similar exposure and slope. The four aspect classes were  $315^\circ - 45^\circ$ ,  $45^\circ - 135^\circ$ ,  $135^\circ - 225^\circ$ , and  $225^\circ - 315^\circ$ , which stood for North, East, South, and West. We tried to pay attention to the pixels with a null (zero) value, which are to be considered towards the South rather than the North as they are painful but in any case conducive to the installation of photovoltaic panels. From  $0^\circ$  to  $90^\circ$ , the 9 slope classes were equally divided into groups of  $10^\circ$ .

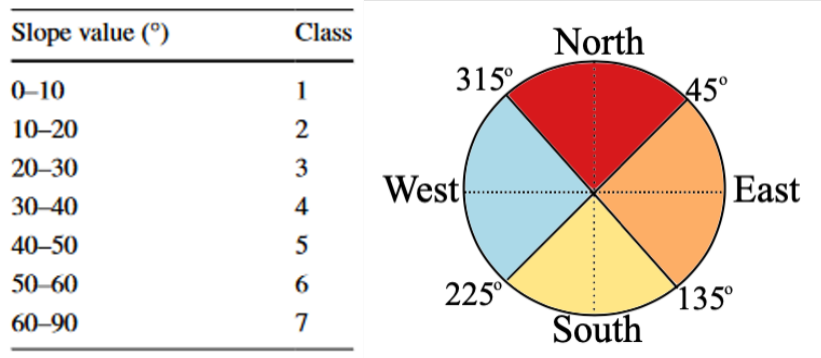


Figure 39 Slope and Aspect

In the instance of the aspect raster, there is an angular direction or bearing where  $0^\circ$  represents the North and each degree is allocated by changing colours until it wraps back around to represent  $360^\circ$ ; in this manner,  $180^\circ$  symbolises the South. Colours are completely random, but they are employed in the most effective way to make them as comprehensible as possible. To identify the directions to the cardinal points, a more colour band was used for the aspect map. Because we are interested in the South (an exposure of 0 means that the slope faces north, 90 turns east, 180 turns south, and 270 turns west), we should focus our attention on the green area, between  $135^\circ$ - $225^\circ$ .

The aspect raster is shown below. The left one represents the aspect of the whole area with all the classes in different colors specified in the legend. On the other hand, the figure on the right demonstrates the area of interest and the useful aspect class together. Green color was selected to specify the South aspect of the raster layer.



*Figure 40 Aspect results for Aosta 2 DSM*

After the aspect raster was created, the second step was creating the slope raster for the spatial analysis. The slope raster is represented in the figure below and it consists of all the rooftops in the Aosta raster. Each pixel of the slope raster is assigned an angle, with  $0^\circ$  indicating a flat rooftop and  $90^\circ$  denoting a steep one. The rasters which have smaller values than 60 were eliminated after the whole dataset was classified. After reclassifying the raster dataset, the layer was masked by using the “r.mask.vect” GDAL tool in order to cancel the roads and trees that are out of interest for the project. A blue gradient was utilised to highlight the form contours of the top half of the building and its inclination with regard to the horizon on the slope map below. The legend highlights the meaning of the colors used in the map layer and the highest slope is specified as dark blue. Other characteristics, including the roof ridges, are also visible as dark blue lines separating the roofs; this indicates that the slope is fast changing in degrees, making the roofs unsuitable for installing solar systems.

Only the flat and south-facing pixels remained after the reclassification; the spots with slopes more than 60 degrees were eliminated as being unsuitable for PV installation. Additionally, they were removed, including information from roads and trees, by using the software's built-in building footprints as it was explained in the workflow.



*Figure 41 Slope results for Aosta 2 metres resolution*

The reclassified and masked slope and aspect rasters that are consisting only the rooftops in Aosta were converted to vector polygons by using the raster conversion tool. This technique enables the creation of polygons to represent each set of neighboring pixels with the same value. Later on, those vector layers were intersected by using the intersection tool. This format is significantly more beneficial since polygons, like lines or dots, may be exported as shapefiles, allowing for the storage of each polygon's shape, height, breadth, and position in addition to any other properties that can be recorded as part of the database file, including slope and aspect.



*Figure 42 Intersection of aspect and slope for Aosta 2*

Roof planes may be identified from these rasters because they generally face in the same direction and have a consistent slope throughout the whole area of the roof plane. Roof planes may be determined by taking the intersection of the aspect polygons (south direction + flat roofs) and the slope polygons (below  $60^\circ$ ) since they share a similar aspect

and a common slope over their surface. A new set of forms with one aspect value and one slope value are produced as a result of this operation; these shapes represent roof planes.

After completing the spatial analysis by creating the slope and aspect rasters and reclassifying them by using the classes assigned and masking them in order to eliminate the areas different from rooftops, polygonising and intersecting the useful areas for solar pv installation the next step was to include the shadow effect by using four days method.

4 days shadow analysis is generated by constructing a shadow pattern for each hour between dawn and sunset, and the solstices and equinoxes were selected as the 4 days to guarantee the whole range of the Sun's positions over a year was taken into account. The particular dates in consideration were March 20, June 21, September 23, and December 22, 2021. The generated shadow rasters were represented below.

The simulations of the shadow analysis were completed by using the “daily shadow analysis” tool included in UMEP toolbox that was mentioned in the methodology section.



*Figure 43 Shadowing rasters for 4 days in 2021*

The hourly shadow rasters from each day were merged to form a continuous binary raster. Dark areas are representing the shadowed areas and the white rasters show the lit areas which were exposed the sun during all those selected four days during the year. Therefore, dark rasters were eliminated by using “r.null” GDAL tool in QGIS and the raster map consisting only lit areas was masked by “r.mask.vect” tool in order to cancel the roads and trees in order to obtain only the lit areas on rooftops to install the PVs. The merged and masked lit areas raster is shown in the figure below. Whilst the left figure demonstrates the whole area where shadow analysis was applied, the right figure shows the rooftops in detail.



*Figure 44 Crossed unique shadow raster (further on the left and zoom on the right)*

After obtaining the lit areas raster by shadow analysis, the “polygonise” tool was used to create polygons of the lit areas. The vector layer consists all the lit areas were used to determine the overall lit area which can also be called as the suitable area for rooftop installation was created and demonstrated below in the figures.



*Figure 45 Vectorized unique shadow results of lit areas*

After completing the spatial and shadow analysis, roof planes created by the aspect and slope polygons were intersected with the lit areas polygons created by shadow analysis. This gives us a clear picture of the ideal overall space for placing PV panels considering the shadowing effect.

The Zonal Statistics tool in the QGIS processing bar, which enables statistical calculations using a vector layer, such as the capability to calculate the area of each extracted polygon, was used to determine the aspect and slope of each plane of the roof.

After managing the spatial and shadowing analysis simulation, our attention shifts to the irradiance simulation. An irradiation simulation is essential because the diffuse component of solar irradiance is heavily influenced by nearby objects like buildings and trees since part of the light bounces and scatters from them. Each pixel contains a color that represents the yearly irradiation at that specific spot, with blue to red denoting low to high irradiation. The output raster is in kWh units, and each pixel represents a 2 m<sup>2</sup> area.

In order to perform the irradiance simulation, the first step was to create wall height and wall aspect rasters by using the DSM of Aosta with 2 metres resolution. The wall aspect and wall height rasters were shown respectively in the figure below consisting of the building footprints demonstrated with the red lights.



*Figure 46 Wall aspect and Wall height results for Aosta 2*

After wall height and wall aspect rasters were obtained, the SEBE analysis was performed by using the DSM, DTM and meteorological dataset of Aosta and the wall height and wall height rasters. The figures below represent the result of the SEBE analysis. The figure on the left is the first result that is non-filtered, and the left figure shows the areas consisting an irradiance higher than 900 kWh since an irradiance smaller

than 900 kWh is not sufficient enough to install solar PVs. Therefore the areas where irradiance is lower than 900 kWh were filtered out by using the “r.null” tool in QGIS.



*Figure 47 SEBE results for Aosta 2*

After the irradiance lower than 900 kWh was nulled, the mask tool was used in order to eliminate the areas different from rooftops. The masked rasters are shown in the figure below.

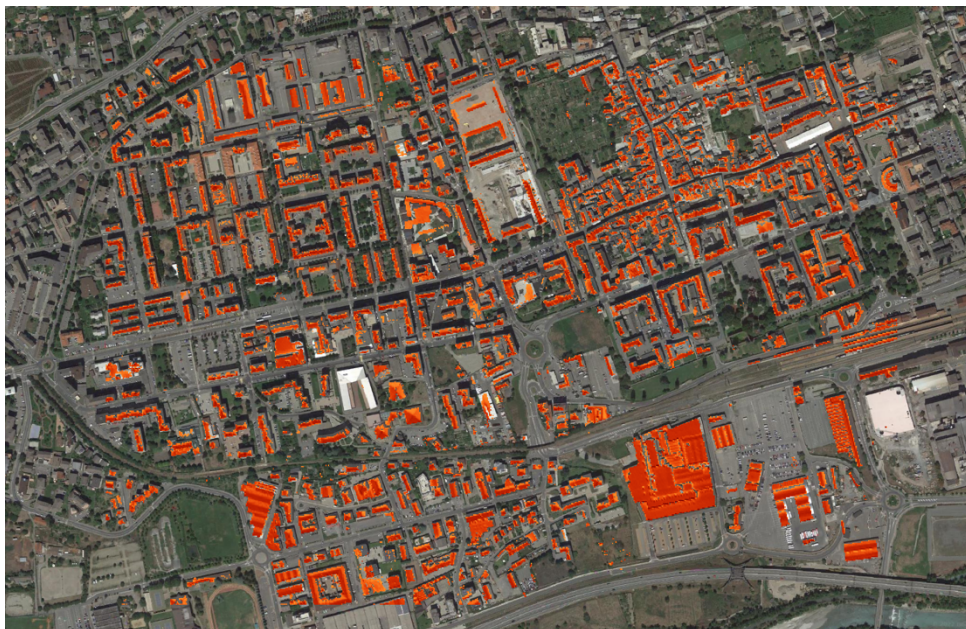


*Figure 48 Final SEBE results for Aosta 2*

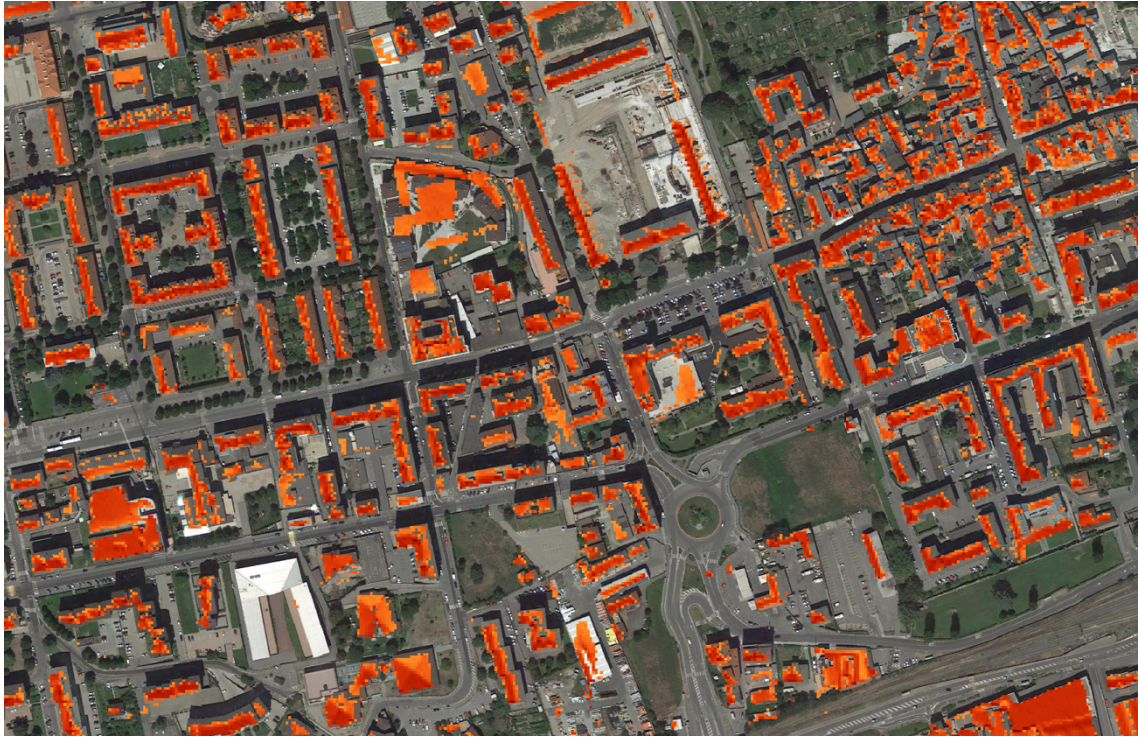


*Figure 49 Final SEBE results in detail for Aosta 2*

SEBE analysis was performed by using the information of spatial and shadow analysis. In order to compare the final SEBE results and the result of the shadow analysis the figure is added below for demonstration of the difference between those two maps.

Many of the polygons found at the point where the vectors cross are merely a few pixels wide or have odd shapes. In order to maintain the original roof designs and remove these odd roof regions, some post-processing is required. This was accomplished using a number of buffering procedures that entail smoothing out the forms by expanding or contracting the shapes through the filters by a certain amount. In the picture, the outcome of these post-processing procedures can be seen after taking into account the need of at least 7 m<sup>2</sup> for every kWp.

The diffuse component of solar irradiance is strongly dependent on the nearby structures, such as buildings and trees, as some of the light reflects and scatters off of them. This necessitates an irradiation simulation. With colors ranging from blue to red denoting low to high irradiation, each pixel has a color that represents the yearly irradiation at that precise position. Each pixel in the output raster corresponds to a 2 m<sup>2</sup> area, and the output raster's units are in kWh.

The "Zonal Statistics" tool in QGIS was used to take advantage of this feature by locating certain crucial data, such as the mean or median of the irradiance levels within each polygon. This yields a computation of the average yearly energy across polygons in kWh/m<sup>2</sup>, a figure that may be used to determine the solar PV system's potential energy production and the ideal location for installation.

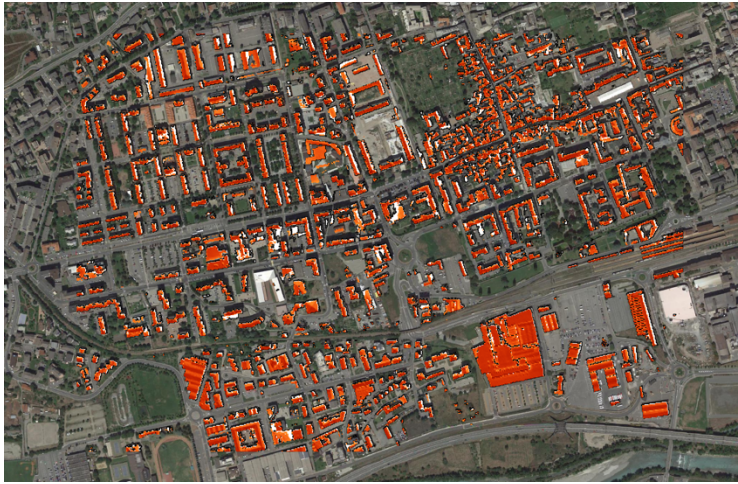


*Figure 50 SEBE and Shadowing analysis comparison*

The white areas are showing the lit areas and the orange areas are the results of the SEBE analysis.

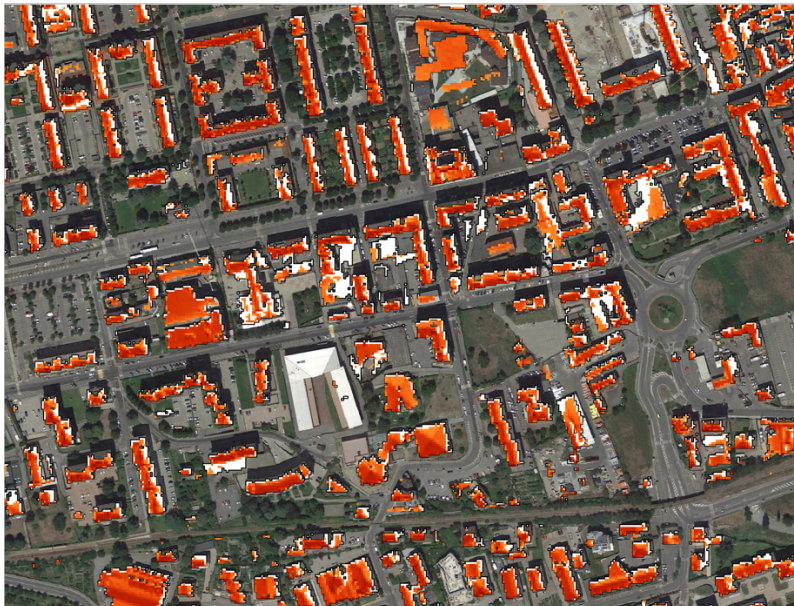


*Figure 51 SEBE and Shadowing analysis comparison in detail*

The difference between the two analyses is seen in the figures above. The numerical results will be given in the table at the end of this chapter.

### **4.3 SEBE and Shadow Analysis for Aosta DSM 0.5**

The DSM of the city of Aosta with a resolution of 0.5 m<sup>2</sup> should also be properly replicated by following all the processes that were just completed for the 2 m<sup>2</sup> resolution held in the previous subchapter. The issue is that because there are so many more parameters to take into consideration on the simulation grid with the equipment we currently have, processing times would rapidly increase. Even for the 2 m resolution it was necessary to tile the project layer. The area selected for analysis of 0.5 m was supposed to be even smaller than the analysis of 2 m resolution.



*Figure 52 Tiled Aosta DSM for 0.5 resolution*



Figure 53 South aspect (between 135-225) maps



Figure 54 South Aspect with building footprints



*Figure 55 Slope and aspect results for Aosta 0.5 DSM*



*Figure 56 Wall height and Wall aspect maps for Aosta 0.5*



*Figure 57 SEBE results for Aosta 0.5*

In the final step, calculate the area after eliminating the wall area from the structures (which is expected to have a slope greater than 60). The amount of energy collected must be economically viable in order to visualise where solar panels should be installed. As irradiation below 900 kWh is regarded as being too low for the generation of solar energy Pixels lower than 900 can be removed using a filter. You can limit visibility to locations that are more interesting than a certain threshold by changing transparency in the properties section of the desired layer.

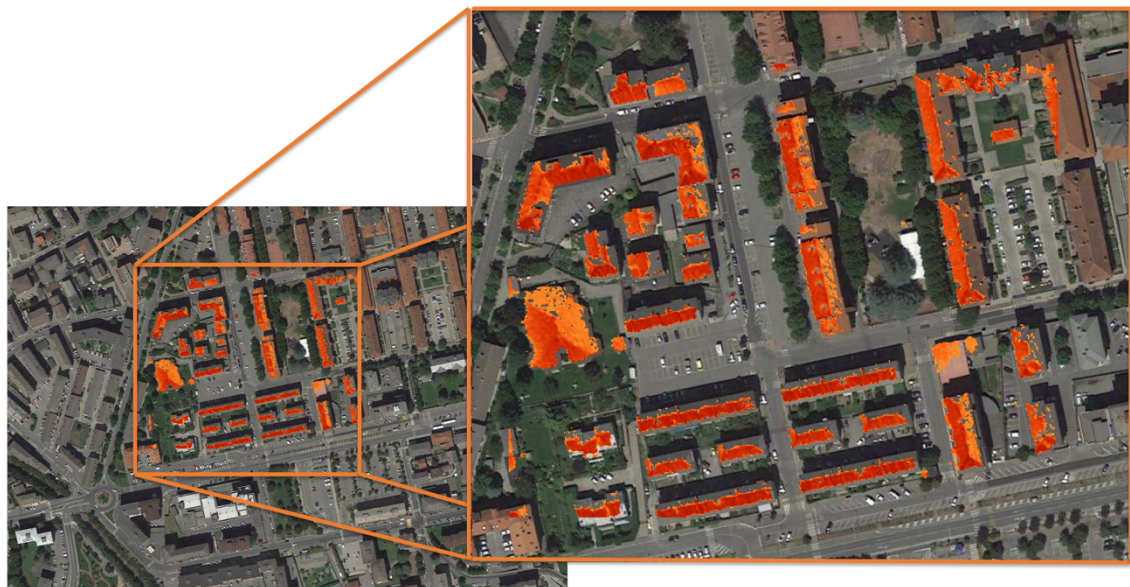


Figure 58 SEBE results for Aosta 0.5 in detail



Figure 59 Shadowing analysis rasters for 4 days

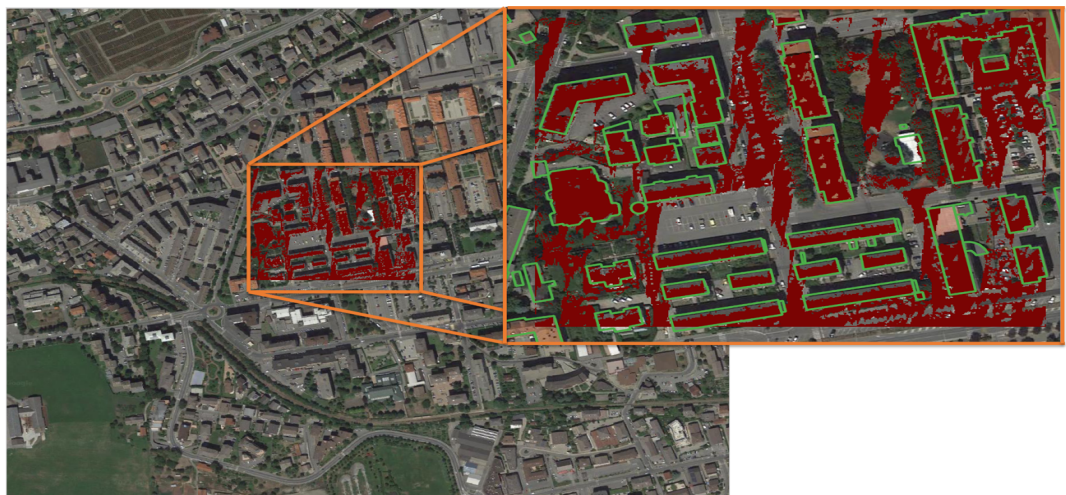


Figure 60 Shadowing analysis result for Aosta 0.5 (Lit Areas)



Figure 61 Lit areas with Building footprint for Aosta 0.5

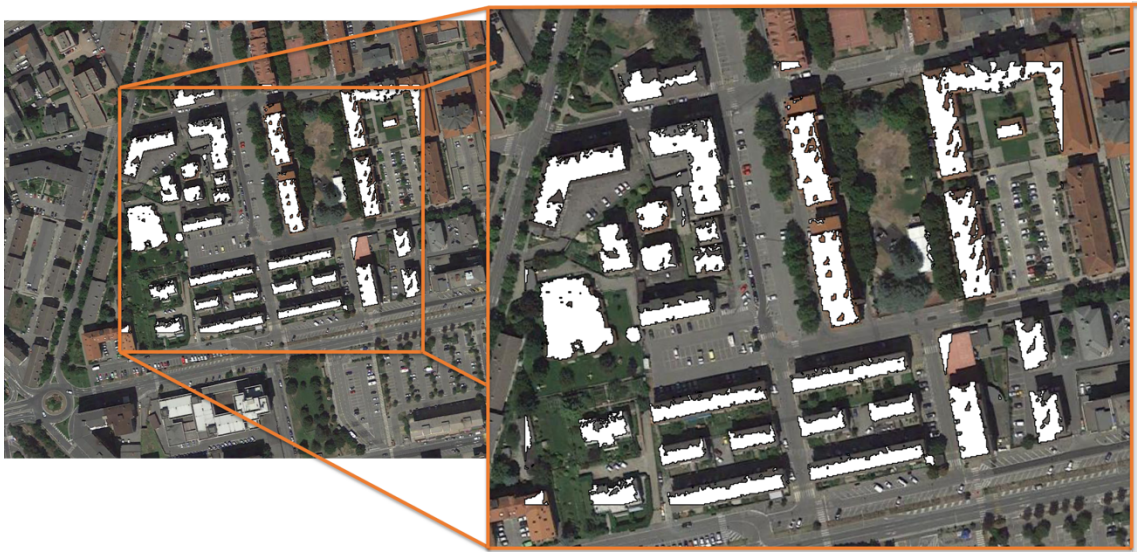


Figure 62 Vectorized lit areas as result of shadowing analysis

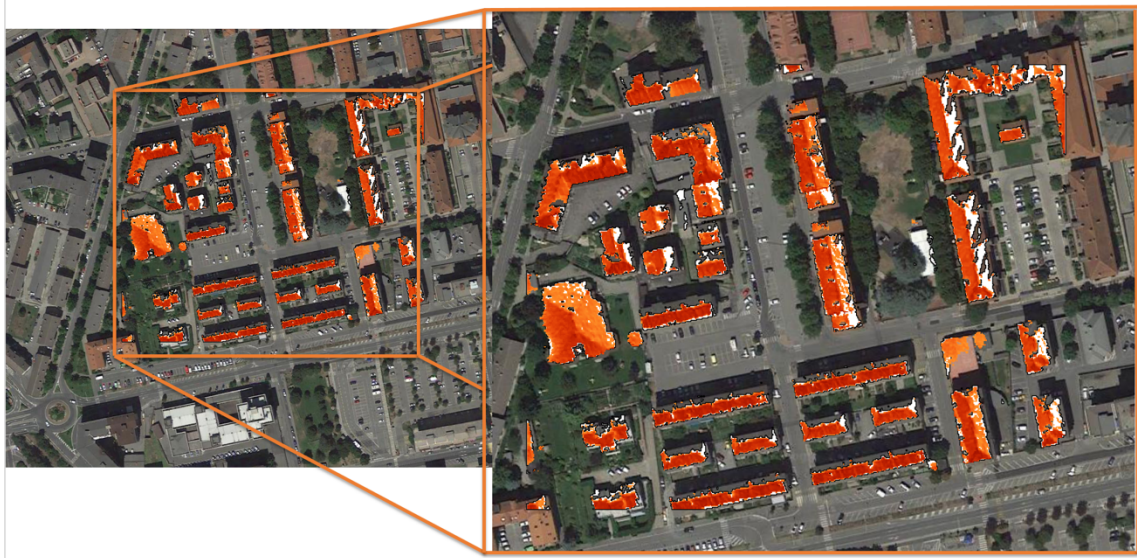


Figure 63 SEBE and shadowing analysis comparison for Aosta 0.5

## 4.4 Indirect method

### 4.4.1 Coefficient for Reduction

Estimating the roof size is a crucial component in understanding a building's solar thermal potential. The available roof area must be calculated after taking into account a number of factors. The Aosta Valley geoportal downloads the reference data that identifies every single building and its footprint and manipulates it on QGIS. The Piedmont region's buildings are entirely represented in this dataset, with their geometries broken down into different categories. Only the civil, social, and administrative buildings, as well as the commercial and industrial ones, are taken into consideration for this study. Since little is known about roofing characteristics, it is necessary to assume a representative roofing typology and conduct an empirical analysis of it based on a visual review of Google Earth images.

The usable roof area that receives solar radiation for the PV facility is defined as the geographic potential for solar photovoltaic installation. Both absolute and relative reductions are undertaken in order to lower the gross surface area to the realistically accessible surface area for solar PV systems. The definitions of these cuts are as follows:[69]

- Absolute reduction entails omitting any structures with particular protections (such as cultural heritage values) or because they were constructed on protected land where PV installations are not allowed by legislation.
- Relative reduction is the process of multiplying the georeferenced layers' calculated total roof area by various utilisation parameters, such as those resulting from orientation, inter-array distance, and other competing applications.

#### 4.4.2 Eligible area estimation for PV installation

The mutual-shading effect is taken into consideration in this analysis since all building roofs are regarded as flat roofs. The inter-array distance design is not straightforward and depends on a variety of variables that are easily adaptable on a case-by-case basis. The covering index coefficient  $C_{COV}$ , which is assumed to be equal to 0,5 and indicates the ratio of module surface divided by the total roof surface available, is included in order to account for these gaps.[24]

As solar collectors are quite effective and practical economically at that latitude, there are already a good number of them on the rooftops of Aosta Valley. Due to the possibility of solar-thermal systems occupying 15% of the roof surface, it is thought that this area may not be used. The corrective solar-thermal coefficient  $C_{ST}$  is therefore considered to be equal to 0,85. As a precaution, it is also taken into account that chimneys, aerials, roof terraces, heating, ventilation, and air conditioning (HVAC) systems, or other functions, occupy 35% of the roofs' area. As a result, the corrective feature coefficient, or  $C_F$ , of value 0,65 is introduced by Bergamasco and Asinari.[24] The total corrective coefficient for roof-top PV plants,  $C_{RF}$ , is produced by adding all the coefficients stated above.[23]

$$C_{RF} = C_{COV} \cdot C_{ST} \cdot C_F = 0,5 \cdot 0,85 \cdot 0,65 = 0,2835$$

$C_{RF}$  limits the total roof area that can be used for solar panels, hence limiting the global PV potential. It shows what percentage of the roof's surface can be covered by solar panels.[23]

## 4.5 Comparison of different resolutions and methods

The proposed multiple technique is then used to the Aosta Valley to assess the technological potential of solar photovoltaic resources, which are acknowledged as the most commercially convenient and established renewable technology. It is possible to estimate the quantity of electricity that could be created by solar panels put on rooftops; an estimate of the nominal power to install to produce the predicted potential energy has also been supplied.

The factors influencing the analysis and their values are listed below:

- Efficiency =  $\eta_{II} \eta_{\eta EE} \cdot AARR = 0.73 * 0.16 = 0.1186$
- $H_g = 1588$  [kWh/m<sup>2</sup>/year] [91]
- Equivalent hours = 992 hours/year
- Reduction factor = 0,2835



Figure 64 The overall suitable rooftop area calculation by eliminating the areas smaller than 7m<sup>2</sup>

The results of the thesis are given in the table below. It can be instantly seen that the yearly electricity consumption and hence potential power alter dramatically when one approach is used instead of another. As it might have been expected, the indirect method, which has been used in many of the articles examined during the literature review, is the one that approximates by excess and overvalues the estimations, as well as the one that does not differentiate the resolution of one method over another. To sum up, it would be the last resource when there are very little data available with modern technology and all resources available.

Table 8. PV Potential Results of Aosta Rooftops

Method	Resolution [m2]	Rooftop Surface [m2]	Yearly Electricity Production [GWh/year]	PV Power [MW]	Self Sufficiency Rate
Shadow Analysis	0.5 x 0.5	5448	1.02	0.92	0.2
Rooftop Segmentation	0.5 x 0.5	3262	0.6	0.54	0.12
Graphical Modeler	0.5 x 0.5	5490	1.03	0.93	0.2
Shadow Analysis	2.0 x 2.0	7727	1.45	1.3	0.27
Rooftop Segmentation	2.0 x 2.0	4965	0.94	0.84	0.18
Graphical Modeler	2.0 x 2.0	8570	1.6	1.45	0.33
Indirect Method	-	10547	2	1.78	0.4

In comparison, the other estimates are quite near to each other and appear to be very accurate. This discrepancy is due to the fact that while working at a higher resolution for roof segmentation, the discovery of more barriers that lesser resolutions may not detect results in a reduction of the total possible rooftop space. On the other hand, it may be remarked that the graphical modeler appears to be more exact since it has the capacity of filtering and buffering the roof region. It has the capacity to integrate and join smaller sections that are less than 7 square meters that would otherwise be deleted in order to create a larger space free of obstacles.

The precision between shadow analysis results and graphical modeler results demonstrates that four days of shadowing analysis would be an accurate solution for estimating the technical potential of solar photovoltaics itself without considering rooftop segmentations.

The self-sufficiency is the ratio of a building's primary energy consumption to primary energy output. Energy production is determined by subtracting the energy necessary for energy production from the energy generated by a new renewable energy system, whereas energy consumption is calculated by adding primary energy consumption and production per unit area. [92]

# Chapter 5

## 5. Improvements and Future Work

In this section, the possible improvements and recommendations for future work are mentioned. This thesis is focused on Aosta Valley and for Aosta Valley all the data are public and can be accessible directly from geoportals. However, if the location of the desired research area changes, the legal procedure should change as well and it should be formally requested for the research purpose. It might take time to receive the exact data one is looking for, and even if the data reliability is high, some improvements can be necessary in assistance.

In the last portion, it was discovered that raising the data resolution strengthened and improved the accuracy of the solar irradiance values. The finer resolution 0.5m raster results are clearly more dependable than the coarse resolution 2m raster findings. The high-resolution difference and its influence on the outcomes were highlighted in the majority of the publications studied throughout the literature study. Therefore, this enhancement has been completed, and the next step may be to apply this strategy to broader regions. Because computing time on personal computers is too long, appropriate technical equipment should be provided for this reason.

Roof segmentation can be done more precisely, and the module placement can be done as future work. Based on this improvement, the economical potential of the rooftops can be estimated as well. Since with the methodologies used in this thesis, the physical, geographical and technical potentials of Aosta Valley were computed considering the shadowing effect and separately with the shadowing analysis. Next step can be estimating the economic potential with a combination of better roof segmentation.

# Bibliography

[1] IPCC (2014), Pachauri, R. K. *et al.* Climate Change 2014: Synthesis Report.

Contribution of Working Groups I, II and III to the Fifth Assessment Report of the Intergovernmental Panel on Climate Change, p. 151, IPCC, Geneva, Switzerland.

[2] IPCC (2018), Summary for policymakers, in *Global warming of 1.5°C an IPCC*

*special report on the impacts of global warming of 1.5°C above pre-industrial levels and related global greenhouse gas emission pathways, in the context of strengthening the global response to the threat of climate change, sustainable development, and efforts to eradicate poverty*, edited by V. Masson-Delmotte, P. Zhai, H. Pörtner, D. Roberts, P. Skea, J. Shukla, A. Pirani, W. Moufouma-Okia, C. Péan, R. Pidcock, S. Connors, J. Matthews, Y. Chen, X. Zhou, M. Gomis, E. Lonnoy, T. Maycock, M. Tignor, and T. Waterfield, p. 32, World Meteorological Organization, Geneva, Switzerland.

[3] UNITED NATIONS, *CLIMATE CHANGE 2021* . .

[4] IEA, “World Energy Outlook 2020,” 2020.

[5] Global Initiative of the United States, “The Sustainable Development Goals,” no. December, 2015.

[6] European Commission, *Proposed Mission : A Climate Resilient Europe* . .

[7] U.S Energy Information Administration, 2019

[8] European Market Observatory for Energy, “Quarterly Report 2021, on European Electricity Markets,” vol. 13, no. 4, 2020.

[9] Sarah Wolf, The European Green Deal- More Than Climate Neutrality, Vol 56, 2021, no:2, pp. 99-107

[10] D. general for E. European Commission, “Annual Activity Report,” 2022.

[11] G. S. E.- GSE, “Copertina RAPPORTO STATISTICO 2017.”

- [12] Gestore Servizi Energetici - GSE, “RAPPORTO STATISTICO 2020 ENERGIA,” 2020.
- [13] Gestore Servizi Energetici - GSE, “Rapporto statistico Solare Fotovoltaico 2021.”
- [14] P. Mavsar, Simplified Method for Analyzing the Availability of Rooftop Photovoltaic Potential, *Energies* 2019, 12(22), 4233, 2019.
- [15] M. M. Hoogwijk, *ON THE GLOBAL AND REGIONAL POTENTIAL OF RENEWABLE ENERGY*, no. november 1974. 2004.
- [16] E. Fakhraian, The Urban Rooftop Photovoltaic Potential Determination, Sustainability 2021
- [17] J. A. D. Deceased and W. A. Beckman, *of Thermal Processes Solar Engineering*, 1999.
- [18] S. Izquierdo, M. Rodrigues, and N. Fueyo, “A method for estimating the geographical distribution of the available roof surface area for large-scale photovoltaic energy-potential evaluations,” vol. 82, pp. 929–939, 2008.
- [19] A. Walch, R. Castello, N. Mohajeri, and J. Scartezzini, “Big data mining for the estimation of hourly rooftop photovoltaic potential and its uncertainty,” *Appl. Energy*, vol. 262, no. November 2019, p. 114404, 2020.
- [20] K. Mainzer, S. Killinger, R. Mckenna, and W. Fichtner, “Assessment of rooftop photovoltaic potentials at the urban level using publicly available geodata and image recognition techniques,” *Sol. Energy*, vol. 155, pp. 561–573, 2017.
- [21] T. Hong, M. Lee, C. Koo, and J. Kim, “Estimation of the available rooftop area for installing the rooftop solar photovoltaic ( PV ) system by analyzing the building shadow using Hillshade analysis,” *Energy Procedia*, vol. 88, pp. 408– 413, 2016.
- [22] E. Jadrake, J. Alegre, G. Martı, and J. Ordo, “Analysis of the photovoltaic solar energy capacity of residential rooftops in Andalusia ( Spain ),” vol. 14, no. 2010, pp. 2122–2130, 2020.
- [23] L. K. Wiginton, H. T. Nguyen, and J. M. Pearce, “Computers , Environment and Urban Systems Quantifying rooftop solar photovoltaic potential for regional renewable energy policy,” *Comput. Environ. Urban Syst.*, vol. 34, no. 4, pp. 345–357, 2010.

- [24] L. Bergamasco and P. Asinari, "Scalable methodology for the photovoltaic solar energy potential assessment based on available roof surface area : Application to Piedmont Region ( Italy )," *Sol. Energy*, vol. 85, no. 5, pp. 1041–1055, 2011.
- [25] L. Bergamasco and P. Asinari, "Scalable methodology for the photovoltaic solar energy potential assessment based on available roof surface area : Further improvements by ortho-image analysis and application to Turin ( Italy )," *Sol. Energy*, vol. 85, no. 11, pp. 2741–2756, 2020.
- [26] M. C. Brito, N. Gomes, T. Santos, and J. A. Tenedo, "Photovoltaic potential in a Lisbon suburb using LiDAR data," vol. 86, pp. 283–288, 2012.
- [27] A. Strzalka, N. Alam, E. Duminil, V. Coors, and U. Eicker, "Large scale integration of photovoltaics in cities," *Appl. Energy*, vol. 93, pp. 413–421, 2012.
- [28] "Lukač et al. - 2013 - Rating of roofs' surfaces regarding their solar po.pdf." .
- [29] J. Peng and L. Lu, "Investigation on the development potential of rooftop PV system in Hong Kong and its environmental benefits," *Renew. Sustain. Energy Rev.*, vol. 27, pp. 149–162, 2013.
- [30] J. A. Jakubiec and C. F. Reinhart, "A method for predicting city-wide electricity gains from photovoltaic panels based on LiDAR and GIS data combined with hourly Daysim simulations," *Sol. Energy*, vol. 93, pp. 127–143, 2013.
- [31] T. Hong, C. Koo, J. Park, and H. S. Park, "A GIS ( geographic information system ) -based optimization model for estimating the electricity generation of the rooftop PV ( photovoltaic ) system," *Energy*, vol. 65, pp. 190–199, 2014.
- [32] "Lukač et al. - 2014 - Buildings roofs photovoltaic potential assessment .pdf." .
- [33] R. Singh and R. Banerjee, "Estimation of rooftop solar photovoltaic potential of a city ScienceDirect Estimation of rooftop solar photovoltaic potential of a city," *Sol. ENERGY*, vol. 115, no. May, pp. 589–602, 2015.
- [34] K. Fath, J. Stengel, W. Sprenger, H. Rose, F. Schultmann, and T. E. Kuhn, "ScienceDirect A method for predicting the economic potential of ( building- integrated ) photovoltaics in urban areas based on hourly Radiance simulations," *Sol. Energy*, vol. 116, pp. 357–370, 2015.

- [35] D. Assouline, N. Mohajeri, and J. Scartezzini, "Quantifying rooftop photovoltaic solar energy potential : A machine learning approach," *Sol. Energy*, vol. 141, pp. 278–296, 2017.
- [36] T. Hong, M. Lee, C. Koo, K. Jeong, and J. Kim, "Development of a method for estimating the rooftop solar photovoltaic ( PV ) potential by analyzing the available rooftop area using Hillshade analysis," *Appl. Energy*, vol. 194, pp. 320–332, 2017.
- [37] D. Assouline, N. Mohajeri, and J. Scartezzini, "Large-scale rooftop solar photovoltaic technical potential estimation using Random Forests," *Appl. Energy*, vol. 217, no. February, pp. 189–211, 2018.
- [38] N. Mohajeri, D. Assouline, B. Guiboud, and A. Bill, "A city-scale roof shape classification using machine learning for solar energy applications," *Renew. Energy*, vol. 121, pp. 81–93, 2018.
- [39] F. Mansouri, K. James, B. Dan, J. Locke, and S. Paul, "Evaluating solar energy technical and economic potential on rooftops in an urban setting : the city of Lethbridge , Canada," *Int. J. Energy Environ. Eng.*, vol. 10, no. 1, pp. 13–32, 2019.
- [40] Song, "An Approach for Estimating Solar Photovoltaic Sensing Images," pp. 1– 14.
- [41] Z. Huang, T. Mendis, and S. Xu, "Urban solar utilization potential mapping via deep learning technology : A case study of Wuhan , China," *Appl. Energy*, vol. 250, no. May, pp. 283–291, 2019.
- [42] H. Alhammami and H. An, "Techno-economic analysis and policy implications for promoting residential rooftop solar photovoltaics in Abu Dhabi , UAE," *Renew. Energy*, vol. 167, pp. 359–368, 2021.
- [43] K. Bódis, I. Kougias, A. Jäger-waldau, N. Taylor, and S. Szabó, "A high- resolution geospatial assessment of the rooftop solar photovoltaic potential in the European Union," *Renew. Sustain. Energy Rev.*, vol. 114, no. August, p. 109309, 2019.
- [44] H. G. Lopez-ruiz, J. Blazquez, and M. Vittorio, "Assessing Residential Solar Rooftop Potential in Saudi Arabia Using Nighttime Satellite Images : A Study for the City of Riyadh," no. June, pp. 1–24, 2019.
- [46] B. Fina, H. Auer, and W. Friedl, "Cost-optimal economic potential of shared rooftop PV in energy communities : Evidence from Austria," *Renew. Energy*, vol. 152, pp. 217–228, 2020.

- [47] T. N. C. De Vries, J. Bronkhorst, M. Vermeer, J. C. B. Donker, and S. A. Briels, "A quick-scan method to assess photovoltaic rooftop potential based on aerial imagery and LiDAR," *Sol. Energy*, vol. 209, no. June, pp. 96–107, 2020.
- [48] A. Gomez-exposito, A. Arcos-vargas, and F. Gutierrez-garcia, "On the potential contribution of rooftop PV to a sustainable electricity mix : the case of Spain University of Seville , Spain," vol. 1, pp. 1–37.
- [49] J. R. Nelson and T. H. Grubestic, "The use of LiDAR versus unmanned aerial systems ( UAS ) to assess rooftop solar energy potential," *Sustain. Cities Soc.*, vol. 61, no. June, p. 102353, 2020.
- [50] T. G. Reames, "Energy Research & Social Science Distributional disparities in residential rooftop solar potential and penetration in four cities in the United States," *Energy Res. Soc. Sci.*, vol. 69, no. June, p. 101612, 2020.
- [51] V. M. Phap, N. Thi, T. Huong, P. T. Hanh, P. Van Duy, and D. Van Binh, "Assessment of rooftop solar power technical potential in Hanoi city , Vietnam," *J. Build. Eng.*, vol. 32, no. June, p. 101528, 2020.
- [52] R. Singh, "Approximate rooftop solar PV potential of Indian cities for high-level renewable power scenario planning," *Sustain. Energy Technol. Assessments*, vol. 42, no. April, p. 100850, 2020.
- [53] H. K. Jacobsen, Integrating the bottom-up and top-down approach to energy-economy modeling: the case of Denmark. *Energy Economics* 1998;20;443-461
- [54] Jason M. Stoker, Evaluation of Single Photon and Geiger Mode Lidar for the 3D Elevation Program, *Remote Sens.* 2016, 8(9), 767.
- [55] <https://www.copernicus.eu/it>
- [56] <https://www.ladybug.tools/>
- [57] Council of Europe Conference of Ministers responsible for Spatial/Regional Planning, "Basic texts 1970-2010," Council of Europe, 2010.
- [58] M. Wegener, "Environment and Planning B," *Planning and Design anniversary issue*, pp. 48-52, 1998.

- [59] F. Lindberg, C. Grimmond, A. Gabey, L. Jarvi, C. Kent, N. Krave, T. Sun, N. Wallenberg and H. Ward, “Urban Multi-scale Environmental Predictor (UMEP) Manual,” University of Reading UK, University of Gothenburg Sweden, SIMS China, 2019. [Online]. Available: <https://umep-docs.readthedocs.io>
- [60] P. Corradeghini, “3DMETRICA,” [Online]. Available: <https://3dmetrica.it/dtm-dsm-dem/> [accessed in May 2022]
- [61] Li, Z., Q. Zhu, and C. Gold. *Digital Terrain Modelling, Principles and Methodology*. Boca Raton, FL: CRC Press, 2005.
- [62] C. Ratti, P. Richens, Raster Analysis of Urban Form, Environment and Planning B: Urban Analytics and City Science, Volume 31, Issue 2, 2004.
- [63] Ratti CF, Richens P (1999) Urban texture analysis with image processing techniques. In: Proceedings of the CAAD Futures99, Atlanta, GA
- [64] Konarska J, Lindberg F, Larsson A, Thorsson S, Holmer B 2013. Transmissivity of solar radiation through crowns of single urban trees—application for outdoor thermal comfort modelling. [Theoret. Appl. Climatol., 1–14](#)
- [65] Lindberg, F., Grimmond, C.S.B., 2011a. The influence of vegetation and building morphology on shadow patterns and mean radiant temperatures in urban areas: model development and evaluation. [Theoret. Appl. Climatol. 105, 311–323](#)
- [66] R. Margolis, P. Gagnon, J. Melius, C. Phillips and R. Elmore, “Using GIS-based methods and lidar data to estimate rooftop solar technical potential in US cities,” *Environmental Research Letters*, vol. 12, no. 7, 2017.
- [67] M. Boz, K. Calvert, and J. Brownson, “An automated model for rooftop PV systems assessment in ArcGIS using LIDAR,” vol. 3, no. 3, pp. 401-420, 2015.
- [68] M. Barton, GRASS GIS 7.8.8dev Reference Manual, <https://grass.osgeo.org/grass78/manuals/r.mask.html> [accessed in July 2022]
- [69] P. Campana, A Gridded optimization model for photovoltaic applications, *Solar Energy* volume 202, pp: 465-484, 2020.
- [70] <https://ec.europa.eu/eurostat> [ accessed in August 2022]

- [71] [https://www.statista.com/statistics-glossary/definition/328/confidence\\_level/](https://www.statista.com/statistics-glossary/definition/328/confidence_level/)  
[accessed in June 2022]
- [72] M. Ehmer, A Comparative Study of White Box, Black Box, and Grey Box Testing Techniques, *International Journal of Advanced Computer Science and Applications* 3(6), 2012.
- [73] Mohd. Ehmer Khan, "Different Approaches to White Box testing Technique for Finding Errors," *IJSEIA*, Vol. 5, No. 3, pp 1-13, July 2011.
- [74] Parida B, Iniyan S, Goic R. A review of solar photovoltaic technologies. *Renew Sustain Energy Rev* 2011;15:1625–36.
- [75] Parida B, Iniyan S, Goic R. A review of solar photovoltaic technologies. *Renew Sustain Energy Rev* 2011;15:1625–36.
- [76] Miles RW, Hynes KM, Forbes I. Photovoltaic solar cells: an overview of state-of-the-art cell development and environmental issues. *Prog Cryst Growth Charact Mater* 2005;51:1–42.
- [77] Priscia Gonçalves Vasconcelos S., Photovoltaic solar energy: Conceptual framework, *Renew Sustain Energy Rev* 2017;74:590-601.
- [78] Goetzberger A, Luther J, Willeke G. Solar cells: past, present, future. *Sol Energy Mater Sol Cells* 2002;74:1–11
- [79] Tyagi VV, Rahim NAA, Rahim NA, Selvaraj JAL. Progress in solar PV technology: research and achievement. *Renew Sustain Energy Rev* 2013;20:443–61.
- [80] Spanggaard H, Krebs FC. A brief history of the development of organic and polymeric photovoltaics. *Sol Energy Mater Sol Cells* 2004;83:125–46.
- [81] Moellering, H., and A.J. Kimerling, 1990, A New Digital Slope-Aspect Display Process, *Cartography and Geographic Information Systems*, 17(2): 151-159.
- [82] <https://www.newport.com/t/introduction-to-solar-radiation> [accessed in August, 2022]
- [83] WANG, Zhifeng. (2019). Chapter 2 - The Solar Resource and Meteorological Parameters, In: WANG, Z. *Design of Solar Thermal Power Plants*. (2019). Cambridge: Academic Press. ISBN 978-0-12-815613-1.

[84] Modeling solar radiation, [cit. 2021-03-21]. Esri. Available online: <https://desktop.arcgis.com/en/arcmap/10.3/tools/spatial-analyst-toolbox/modeling-solar-radiation.htm>, 2021.

[85] HOFIERKA, J., SURI, M. (2002): The solar radiation model for Open source GIS: implementation and applications. *Open source GIS - GRASS users conference 2002*. Trento, Italy.

[86] Moran, Joseph M. *Weather Studies: Introduction to Atmospheric Science*, 5th Ed. Boston, MA: American Meteorological Society, 2012.

[87] POLIDORI, L., HAGE, M. E. (2020). Digital Elevation Model Quality Assessment Methods: A Critical Review. *Remote Sens*, 12(32), p. 3522. doi:10.3390/rs12213522

[88] <https://epsg.io/23032-1450> [accessed in August, 2022]

[89] WALD, Lucien, *Basics in Solar Radiation At Earth Surface*. Paris: HAL Id: hal-01676634, 2018.

[90] [www.ametsoc.org/amsedu](http://www.ametsoc.org/amsedu) , “American Meteorological Society Education Program” [accessed in August, 2022]

[91] SolarGis, “Yield assessment of the photovoltaic power plant,” vol. 51, no. February, pp. 1–4, 2018.

[92] Mun, J.H.; Kim, J.C. A Study on the Improvement of Energy Self-Sufficiency Rate for Obtaining Zero Energy Building Certification. *J. Kor. Inst. Illum Electr. Install. Eng.* 2018, 32, 27–32.

